Quantifying the role of reservoirs in altering phosphorus dynamics using a combination of data analysis and process modeling

by

Tori Grootjen

A thesis
presented to the University of Waterloo
in fulfillment of the
thesis requirements for the degree of
Master of Science
in
Earth Science (Water)

Waterloo, Ontario, Canada, 2022

Author's Declaration

This thesis consists of material all of which I authored or co-authored: see Statement of Contributions included in the thesis. This is a true copy of the thesis, including any required final revisions, as accepted by my examiners.

I understand that my thesis may be made electronically available to the public.

Abstract

Excess phosphorus (P) from agricultural watersheds promotes eutrophication in downstream aquatic systems. Reservoirs retain P generated from farm fields and protect downstream waters. Reservoirs also act as hotspots for P transformation, as anoxic conditions can facilitate the release of stored P from the lake sediments. The role of inland reservoirs in P speciation at the watershed scale is relatively unexplored. This problem is growing in importance as approximately half of the global river volume is at least moderately impacted by damming, and is projected to reach 93% with all the planned or proposed dams (Grill et al. 2015). Here we use a decade of soluble reactive P (SRP) and total P (TP) concentration data at the inlet and outlet of two reservoirs, Belwood Reservoir and Conestogo Reservoir, in the Grand River Watershed, Canada. The annual SRP and TP percent retention varied at both reservoirs, showing that the reservoirs acted as a sink in some years and as a source in other years. The percent TP retention in Belwood Reservoir varies from -40% to 32%, while percent TP retention in Conestogo Reservoir is generally lower, between -72% to 25%. The SRP retention in Belwood Reservoir varied between -68% and 43%, while SRP retention in Conestogo Reservoir varied between -71% and 28%. Interestingly, the source-sink behaviour is visible for both SRP and TP and they are similar between years. That is, in years that Belwood Reservoir acts as a source of TP, the reservoir often acts as a source of SRP too. At the seasonal scale, we found that both reservoirs increase the proportion of bioavailable P (SRP:TP ratio) from inlet to outlet between April and October. We then built a process-based model to examine the P cycling and sediment-water interactions controlling this speciation of P in the Belwood Reservoir. The model was able to capture downstream SRP export with NSE_{SRP} = 0.57-0.86 and TP export with NSE_{TP} = 0.60-0.91. The model had difficulty capturing the SRP:TP magnification from inlet to outlet and sediment P accumulation, especially for the first few years of model simulation (2007 - 2012). Model results highlight the role of internal loading during the summer months. As dam construction is on the rise globally, it is critical to understand the impact of reservoirs on the relative reactivity of P in order to mitigate nuisance and potentially harmful algal blooms.

Acknowledgements

I would like to thank the Global Water Futures (GWF) project for providing me with financial support throughout my entire degree. I am grateful for the opportunity to learn and contribute to the project with little worry over finances.

First and foremost, I would like to thank my supervisor, Nandita Basu, for taking a chance on a young woman from the math department and adding me to her incredible lab. I would also like to thank Ruchi Bhattacharya, who assisted with paleolimnology expertise. I greatly appreciate having so many smart women around me as role models.

I am so grateful to have been in a lab that is full of high-quality people who were always willing to share some knowledge, support, laughs and baked goods.

My whole experience at the University of Waterloo would not have been the same without finding my people in the squash community. I'd like to thank Marisa Seth for completely changing my life by introducing me to the squad, my other coaches (Vinit Kudva and Clive Porter), and every teammate I met along the way.

I'd also like to thank my parents for always supporting me in multiple ways. Everything you've done for me does not go unappreciated.

Lastly, a huge thank you to my partner, Cameron Seth, for being a persistent sounding board and source of support.

Dedication

I'd like to dedicate this thesis to Bobby. For being a good boy.

Table of Contents

List of Figures

List of Tables

1.0 Introduction

1.1 Eutrophication and human perturbations of the P cycle

Eutrophication of coastal and freshwater systems has significant environmental, social and economic impacts (Cordell et al. 2009, Elser 2012, Yuan et al. 2018). The eutrophication of a water body occurs from excessive inputs of nutrients, primarily phosphorus (P) and nitrogen (N). The excess nutrients stimulate algal growth, which depletes dissolved oxygen (Wetzel 1983), and creates hypoxic conditions ("dead zones") that contribute to fish kills (Scavia et al. 2014). The resulting algal blooms can also produce toxins that are harmful to humans and aquatic species, and pose risks to drinking water and recreational use (Carpenter et al. 1998). Decline in ecosystem biodiversity, restriction of recreational use, and degradation of drinking water quality are some of the adverse impacts of eutrophication.

Phosphorus is the primary contributor to the eutrophication of many freshwater aquatic systems, being the limiting factor in the production of phytoplankton (Schindler 1978). The primary source for phosphorus is phosphate rock. Humans have exploited this natural source and mined phosphate rock for use in crop production, animal feed, and fertilizers, thus dramatically altering the natural P cycle. In fact, humans have tripled P mobilization from lithosphere to ecosystems globally (Yuan et al. 2018). Eventually, some of this P ends up in lakes and reservoirs and contributes to eutrophication.

External sources of P to water bodies include both point and nonpoint sources. Point sources include industrial and municipal wastewater treatment plants, septic systems, industrial effluent, and atmospheric deposition. Nonpoint sources include streambank erosion of phosphate rock, runoff from forested lands, and runoff of fertilizer or manure applied to croplands or pasture lands (Cordell et al. 2009). The external sources of P mentioned above are well known, whereas the internal source of P, legacy P, is less quantified but can also contribute to eutrophication (Pettersson 1998, Nürnberg 2009). This legacy P has accumulated in the lake sediment from years of fertilizer overapplication. Of the fertilizers applied to agricultural croplands, only 20-30% of P is exported from the watershed (by streams or removed by crop uptake) and the remainder is stored as legacy P within the watershed in soil, lake sediments, groundwater, and wetlands (Nürnberg 2009, Sharpley et al. 2013, Jarvie et al. 2013a). It has been estimated that net P storage in terrestrial and freshwater systems has increased by more than 75%

since preindustrial times (Bennett et al. 2001). Of the P mined by humans, a large portion is applied to agricultural fields for crop production where it accumulates in the soil (Bennett et al. 2001), increasing soil P stores by approximately 7 Tg/yr globally (Yuan et al. 2018). Some of this P applied to agricultural fields is then transported by runoff and accumulates in the sediment of lakes or reservoirs. This accumulated P in soil and lake sediment can be remobilized to increase internal loading and delay downstream water quality improvements (Paerl et al. 2011, Sharpley et al. 2013, Jarvie et al. 2013b, Muenich et al. 2016, Schindler et al. 2016, Ho et al. 2019). This internal source of P, combined with external sources of P, contribute to the eutrophication of lakes and reservoirs.

1.2 Policy context in the Lake Erie Basin

Lake Erie, one the five Great Lakes, bordering US and Canada, has seen recurring eutrophication, harmful algal blooms, and increasing hypoxia (International Joint Commission and International Joint Commission 2014, Scavia et al. 2014, Kane et al. 2014, Watson et al. 2016). In response to algal blooms in the 1970s, the Great Lakes Water Quality Agreement (GLWQA) was signed in 1972 to limit P loading from major municipal sewage treatment plants (International Lake Erie Water Pollution Board et al. 1969). Significant effort has been made to remediate watersheds that drain into Lake Erie. Regulatory measures have been taken to reduce P in laundry and dish detergents, wastewater treatment plants have been upgraded, and a range of best management practices (BMP) have been implemented to reduce P runoff from agricultural fields. As a result of these efforts, Lake Erie saw improvements in water quality in the 1980s (De Pinto et al. 1986, Makarewicz and Bertram 1991, Kane et al. 2014, Schindler et al. 2016). Lake Erie was deemed a success story by a number of eutrophication indicators, until the 1990s when algal blooms returned (Budd et al. 2001, Ouellette et al. 2006, Scavia et al. 2014, Kane et al. 2014). One theory is the “nearshore phosphorus shunt” where it is hypothesized that invasive dreissenid mussels retain P in the nearshore benthic environment, thereby supplying P to benthic algae. Other theories as to why trophic-status changes were observed in Lake Erie, including that the form of P and internal loading of P were not considered in management plans (Kane et al. 2014, Song et al. 2017).

One of the reasons behind the re-eutrophication of Lake Erie is an increase in bioavailable P (Baker et al. 2014), despite the loading of total phosphorus remaining within

limits mandated by the GLWQA (Dolan 1993, Dolan and McGunagle 2005). This increase in the fraction of bioavailable P (soluble reactive P) is suspected to be caused by intensification of agricultural practices, land use changes, and increased runoff (Richards et al. 2010, Joosse and Baker 2011, Sharpley et al. 2013, Michalak et al. 2013, Jarvie et al. 2013a).

Recent studies have also highlighted the role of reservoirs in increasing the fraction of bioavailable P from watersheds. In a study of 200 water quality stations across the Great Lakes Basin, Van Meter et al. (2020) found evidence of increasing proportions of bioavailable P during the summer months in water quality stations downstream of reservoirs. This might be a function of the release of legacy P from reservoir sediments (Orihel et al. 2017). However, still little is known about how reservoirs may magnify bioavailable P, as a function of climate, season and management controls. While internal loading of P in reservoirs has been studied, the implications on watershed scale P fluxes is relatively less well understood (Orihel et al. 2017).

1.3 Phosphorus cycling in reservoirs

The damming of streams turns sections of primary conduits for nutrient transport into lentic environments capable of nutrient storage (Winton et al. 2019). Once trapped in a lake or reservoir, phosphorus is cycled through species pools by various biogeochemical processes. The flux of P from one pool to another depends largely on the size of the source pool and other properties (e.g., redox potential, temperature, pH) that vary seasonally. The main processes that drive the transformation of P within a reservoir are sedimentation and remobilization, sorption and desorption, and mineralization and uptake (Maavara et al. 2015).

Sedimentation and remobilization: Sedimentation is the settling of particulate matter, including particulate P, to lake sediments. Sedimentation occurs when the gravitational pull of particulates is greater than the upward buoyancy forces. The mass flux of P to the sediment is dependent on the total mass of particulate P in the water-column (Porcalová 1990, Hupfer and Lewandowski 2008). Net P sedimentation is gross P sedimentation minus remobilized P. Remobilization is the release of P that was previously chemically bonded (released through dissolution) or adsorbed to lake sediment (released through desorption) (Boström et al. 1982). The main P mobilization process is through redox-controlled release where reactive P is released from iron phosphate complexes ($FePO_4$) in the sediment under anoxic conditions (Boström et al. 1982). Thus, internal loading can be accelerated under anoxic conditions (Nürnberg 1984, Paerl 1988) and can be

influenced by biological variables (Song and Burgin 2017). For this reason, the flux of P from sediment to the water-column depends on the seasonally-dependent hypolimnetic redox potential, stratification and mixing regimes.

Sorption: Sorption processes control the exchange of P between soluble reactive P (SRP) and exchangeable P (EP). Adsorption is the process by which dissolved P attaches to a particle surface and becomes exchangeable P. Desorption is the release of P from oxides, clay minerals or organic matter as EP to SRP. The adsorption and desorption of P from particles occurs in both the water column and lake sediment. Adsorption of dissolved phosphate to iron molecules is stronger under oxic conditions and under anoxic conditions the phosphate desorbs from particles into pore water SRP (Ku et al. 1978, Katsev et al. 2006). As a result, anoxic hypolimnetic conditions increase the rate of desorption and can lead to elevated amounts of reactive P in the water column.

Mineralization and uptake: Mineralization and uptake control the movement of P between the biotic and abiotic pools. Since P is often the limiting nutrient in freshwater lakes, any bioavailable P is used immediately for primary production (Rigler 1956, 1964). Assimilation or uptake of P for primary productivity leads to the transformation of SRP to particulate organic P (POP). Mineralization is the process in which P is transformed from POP to SRP. Mineralization occurs in the water column through the process of releasing P that was previously stored in organisms when they die, as well as in lake sediment from processes driven by soil microbes. Mineralization and uptake rates fluctuate seasonally due to differences in water temperature and stratification regimes (Halemejko and Chrost 1984, Brzáková et al. 2003).

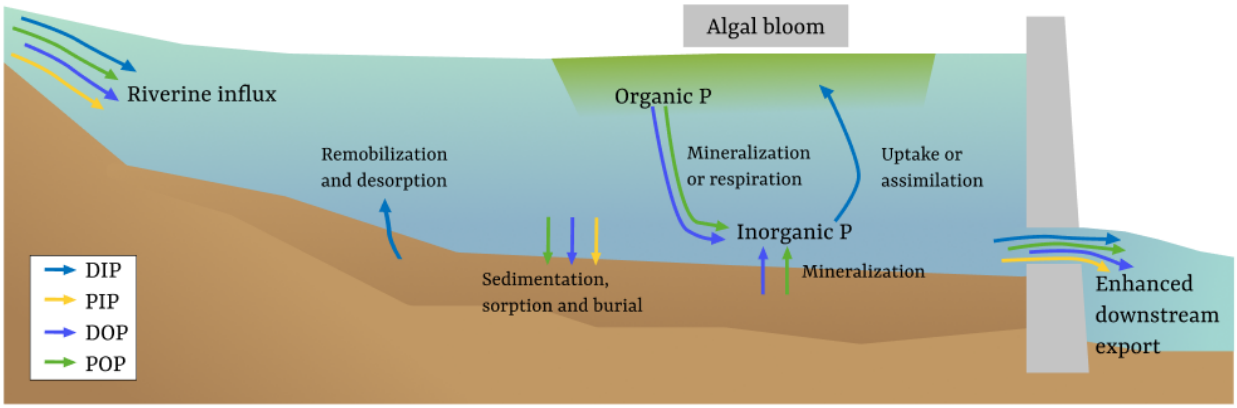

Figure 1. Cycling of phosphorus in reservoirs and the main biogeochemical processes in play. Modified from (Maavara et al. 2020).

1.4 Effect of reservoirs on P speciation at the watershed scale

Reservoirs can act as sources or sinks of P, with the source-sink function changing seasonally (Powers et al. 2015, Orihel et al. 2017, Shaughnessy et al. 2019). Powers et al. (2013) studied long-term river export of TP within 54 catchments in WI, USA and found evidence of TP retention within lakes or reservoirs. They also found that lakes and reservoirs stabilized the seasonal variability in export and introduced time lags in P export (Powers et al. 2013). Reservoirs studied in the mid-western US were found to vary in their TP retention, with multiple systems exhibiting net P export (Powers et al. 2015). Gaining more attention lately is the importance of not only TP, but more bioavailable forms of P (Joosse and Baker 2011, Baker et al. 2014). For example, in a study of more than 200 stations across American and Canadian watersheds,Van Meter et al. (2020) found that seasonal SRP regimes may be strongly impacted by the presence of reservoirs. Reservoir sediments preferentially store particulate P, resulting in higher fractions of SRP being released downstream (Salvia-Castellvi et al. 2001, Donald et al. 2015).

Reservoir sediments can act as P sources under anoxic conditions that often arise from stratification (Hupfer and Lewandowski 2008). When reservoirs thermally stratify in the summer, the hypolimnion can become oxygen deficient from the lack of mixing with the oxygen-rich surface layer. Reducing conditions lead to the release of dissolved P from the sediments to the water column (Molot et al. 2014, Orihel et al. 2017). Studies have found that climate change can cause reservoirs to stratify earlier in the season (Hondzo and Stefan 1991)

and experience less frequent mixing events (Woolway and Merchant 2019). Additionally, the management of a reservoir has the potential to influence the magnitude of such internal loading. The relative impact of climate and management controls on the magnitude of magnification of SRP at a watershed scale remains poorly understood.

1.5 Reservoir P Models

Many models have been built for use in studying phosphorus cycling within lakes and reservoirs. For example, Maavara et al. (2015) built a reservoir P model to study annual P retention in reservoirs at the global scale. However, one limitation of some reservoir P models is the lack of water-column and sediment P coupling. Another P cycling model, the MyLake model, has been used to study daily vertical distribution of lake properties including phosphorus-phytoplankton dynamics and sediment-water interactions (Saloranta and Andersen 2007). However, lake models built to simulate phosphorus retention may not be suitable for reservoirs because of the difference in sedimentation rates, lake/reservoir depth, and water residence time (Hejzlar et al. 2006). Thus, reservoir-specific models are needed in order to study P cycling within reservoirs. Rather than using these off-the-shelf models, we chose to build a flexible, parsimonious model that we could use to ask what role legacy P and today's external P loading have on P speciation dynamics and sediment P accumulation in a reservoir. Not many other reservoir models have been used to study P speciation dynamics and legacy P accumulation over time.

2.0 Research Objectives

The overall goal of this thesis is to study how reservoirs alter the seasonal patterns in P dynamics in watersheds. Specifically this research will:

1. Quantify the effect of reservoirs on seasonal and annual P speciation using data analysis.
2. Create a model to capture both P speciation over time and legacy P accumulation.

To address Research Objective 1, I have analyzed two multi-purpose reservoirs in the Grand River Watershed in Southern Ontario: Belwood and Conestogo Reservoirs. The reservoirs were chosen since they have available climate data, concentration and discharge data at both the inlet(s) and outlet, and have been experiencing annual algal blooms in recent years (2016-2019).

For Research Objective 2, I have used Belwood Reservoir, as a case study for the model application. Due to time constraints, the model was not applied to Conestogo Reservoir.

3.0 Methods

3.1 Study Areas

To study the effect of reservoirs on seasonal P speciation (Research Objective 1), data for two reservoirs in southwestern Ontario was analyzed. Belwood Reservoir is located along the Grand River near Fergus, Ontario and Conestogo Reservoir is located along Conestogo River near Glen Allen, Ontario (**Figure 2**). The reservoirs were built for flood management and low-flow augmentation and are managed for such by the Grand River Conservation Authority (GRCA) (Boyd and Shifflett 2016). The reservoirs are filled by spring rainfall and snowmelt, drawn down during the summer, and collect runoff from fall rainfall. For both Belwood and Conestogo Reservoirs, the dominant upstream land use is agricultural, draining 834 km^2 and 625 km^2, respectively (Loomer and Cooke 2011, GRCA 2017). The height of the dams at Belwood and Conestogo are 22.5 meters and 23.1 meters, respectively (*State of the Watershed Report* 1998).

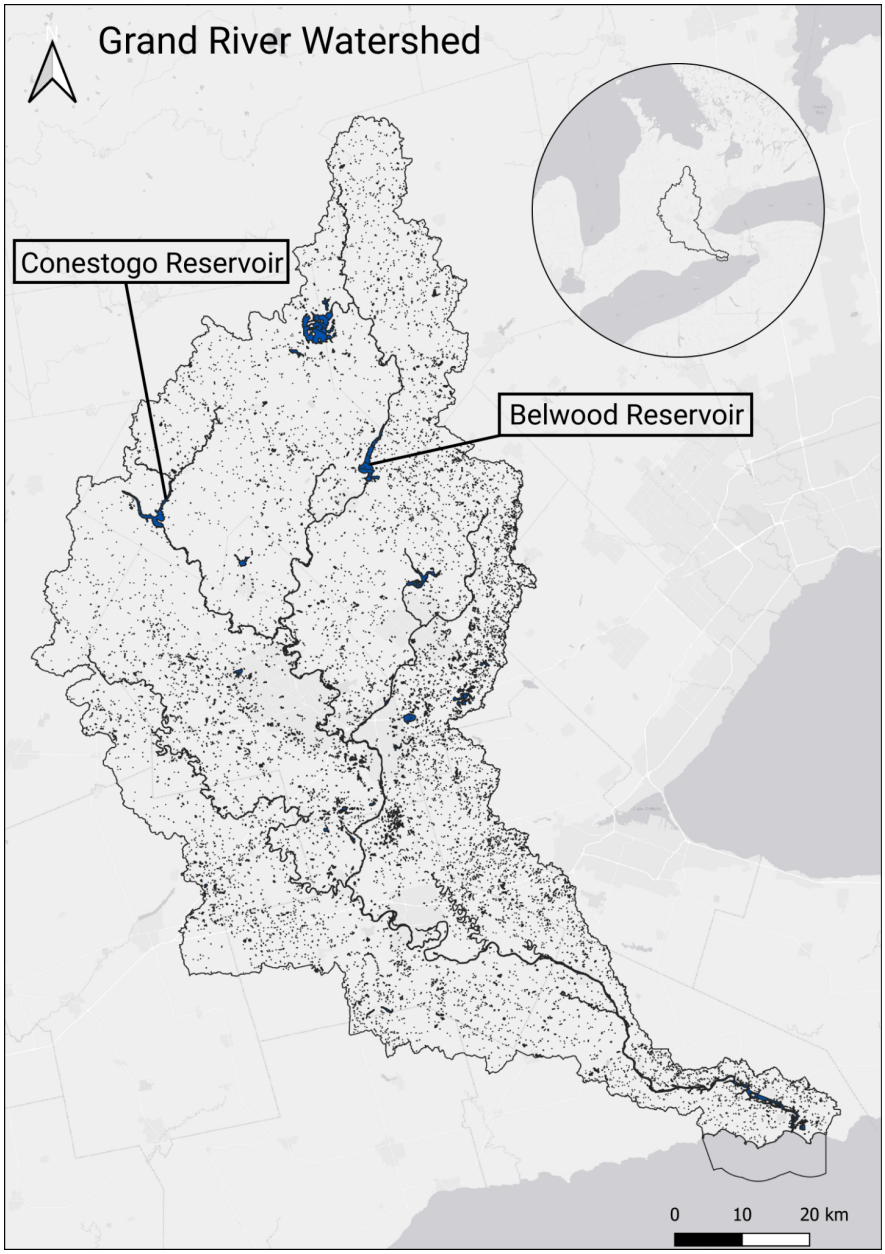

Figure 2. Belwood and Conestogo Reservoirs, located in the Grand River watershed in Ontario, Canada.

3.2 Data Sources and Analyses

3.2.1 Data Sources

I obtained long-term streamflow data and water quality (SRP and TP concentration) (2007-2019) from various local, provincial and national data sources (**Table 1**). Streamflow data was obtained from the Water Survey of Canada (WSC; station IDs included in **Table 1**) (Canada

2007) over the full time period (2007-2019). For one of the inlets to Conestogo Reservoir (inlet 2 at Moorefield), the WSC does not have a discharge station so discharge data was obtained from GRCA's Grand River Information Network ("GRIN" 2020) website (see **Table 1** for station IDs). At the other inlet to Conestogo Reservoir (inlet 1, Conestogo River above Drayton), discharge data from WSC was used when available from 2007-2019, but one gap in data (from Jan 1, 2016 to Mar 3, 2017) was filled by data from the GRIN. The primary source for long-term TP and SRP concentration data was the Provincial Water Quality Monitoring Network (PWQMN 2018) that reported concentrations at the inlet(s) and outlet at both reservoirs over the studied time period, 2007-2019 (see **Table 1** for station IDs). Supplemental winter SRP and TP concentration data came from two studies conducted by GRCA (internal data obtained via personal communication). The first study, Upper Grand River Basin Characterization Study, was conducted between 2010-2018 at the inlet and outlet of Belwood Reservoir. The second study, the Upper Conestogo River Basin Characterization Study, was conducted between 2016-2018 at the inlets and outlet of Conestogo Reservoir. The data from these two studies was aggregated with PWQMN data for Belwood Reservoir and Conestogo Reservoirs, respectively. Both studies provided valuable winter concentration measurements.

Reservoir volume data was obtained for use in the water balance analysis. Measured daily reservoir volume data for 2007-2019 was obtained from GRCA (personal communication, see **Table 1** for station IDs). Measured daily precipitation for both reservoirs for the full time period (2007-2019) was obtained from GRCA (personal communication, see **Table 1** for station IDs). Daily air temperature data was obtained from Environment Canada for Belwood Reservoir (see **Table 1** for station ID), and from GRCA (personal communication) for Conestogo Reservoir. Maximum reservoir surface areas, used in the conversion of evaporation and precipitation, were obtained from GRCA 2018 (*Belwood and Conestogo Water Management Reservoirs* 2018).

Model development for Belwood reservoir required the estimation of inputs from the septic system. Belwood Reservoir is surrounded by both seasonal (May to October) and permanent (year-round) buildings that contribute to septic inputs to the reservoir. The septic inputs from these sources were estimated using data that was compiled in a GRCA report (*Belwood and Conestogo Water Management Reservoirs* 2018). The report estimated contribution from septic systems using conservative estimates of loading (per capita) multiplied by the average number of persons in each building. For the large subsurface sewage discharge

systems (LSSDS), the conservative P load was estimated as the product of the system's capacity and the assumed effluent TP concentration of 9 mg/L. This led to estimates of 876 kg/yr and 1295 kg/yr of phosphorus, respectively, for the year-round and seasonal occupants. Here, we assume that the estimate of loading from surrounding septic systems is consistent for all years. We also assume that the phosphorus contribution from septic systems is in a soluble reactive form.

Table 1. Data sources and station IDs

Data Type	**Sources**	**Belwood Station IDs**	**Conestogo Station IDs**	**Units of Data**
Inlet discharge	Water Survey of Canada (WSC), 2007-2019	02GA014, (43.8617, -80.2722)	Inlet 1: "Conestogo River above Drayton", 02GA039, (43.7833, -80.6378)	m^3/s
	GRCA's GRIN, 01/01/2016-03/31/2017		Inlet 1 supp.: "Drayton" 14913, (43.7833, -80.6378)	m^3/s
	GRCA's GRIN, 2007-2019		Inlet 2: "Moorefield" 14918, (43.7580, -80.7489)	m^3/s
Inlet SRP and TP concentrations	Provincial Water Quality Monitoring Network (PWQMN), 2007-2019	16018406702, (43.8617, -80.2724)	Inlet 1: 16018407502, (43.7569, -80.6700)	mg/L
	Provincial Water Quality Monitoring Network (PWQMN), 2007-2019		Inlet 2: 16018409102, (43.7575, -80.7489)	mg/L
	GRCA, Upper Grand Characterization Study, 2010-2018	1364002, (43.8618, -80.2725)		mg/L
	GRCA, Upper Conestogo River Basin Characterization Study, 2016-2018		Inlet 1: 4393001, (43.7569, -80.6700)	mg/L
	GRCA, Upper Conestogo River Basin		Inlet 2: 4394005,	mg/L

	Characterization Study, 2016-2018		(43.7575, -80.7489)	
Input SRP from septic	(*Belwood and Conestogo Water Management Reservoirs* 2018)	Estimated for surrounding camps and cottages		kg/yr
Outlet discharge	WSC, 2007-2019	02GA016, (43.7308, -80.3408)	02GA028, (43.6547, -80.7019)	m^3/s
Outlet SRP and TP concentrations	PWQMN, 2007-2019	16018403702, (43.7247, -80.3439)	16018407702, (43.6547, -80.7019)	mg/L
	GRCA, Upper Grand River Basin Characterization Study, 2010-2018	2366014, (43.7249, -80.3439)		mg/L
Reservoir volume	GRCA, personal communication, 2007-2019	N/A	N/A	1000 m^3
Precipitation	GRCA, personal communication, 2007-2019	N/A	N/A	mm
Air temperature	Environment Canada, 2007-2019	6142400		℃
	GRCA, personal communication, 2007-2019		N/A	℃

3.2.2 Estimating seasonal loads from sparse concentration data using the weighted regression on time, discharge and season (WRTDS) method

Concentrations of SRP and TP at the reservoirs' inlets and outlets are measured only a few times during the year. To address the data gaps, I have used the weighted regression on time, discharge and season (WRTDS) (Hirsch et al. 2010) method to interpolate between intermittently measured values and estimate daily concentrations. WRTDS estimates concentration using daily measured discharges via this equation:

(1) $$ln(c) = \beta_0 + \beta_1 t + \beta_2 ln(Q) + \beta_3 sin(2\pi t) + \beta_4 cos(2\pi t) + \varepsilon$$

where

c is concentration [ML^{-3}]

β_0, β_1, β_2, β_3, β_4 are fitted regression coefficients

Q [L^3T^{-1}] is daily discharge

t [T] is time

ε is an error term

Data observations greater than four standard deviations were considered to be outliers and were removed from the datasets. Default values for model parameters (half-window sizes) were used. Model fit was analyzed using multiple indicators such as Kling-Gupta Efficiency and R^2 which are summarized in **Table 2**. Modeled and measured concentrations are shown in **Figure 13 and 14**.

Monthly fluxes of SRP and TP at the inlets and outlets were estimated using WRTDSKalman. Using WRTDSKalman resulted in confidence intervals that could be used for the estimate of uncertainty whereas WRTDS does not provide that.

Table 2. WRTDS Error Metrics

Station	**Inlet of Belwood Reservoir**	**Outlet of Belwood Reservoir**	**Inlet 1 of Conestogo Reservoir**	**Inlet 2 of Conestogo Reservoir**	**Outlet of Conestogo Reservoir**
NSE_{SRP}	0.43	0.16	0.55	0.46	-0.17
NSE_{TP}	0.54	0.33	0.64	0.51	0.17
KGE_{SRP}	0.64	0.42	0.77	0.72	0.12
KGE_{TP}	0.70	0.41	0.80	0.70	0.30
$Slope_{SRP}$	0.86	0.86	0.89	0.82	0.80
$Slope_{TP}$	0.9	0.9	0.9	0.89	0.91
R^2_{SRP}	0.60	0.52	0.65	0.59	0.44
R^2_{TP}	0.66	0.59	0.71	0.65	0.54
$PBIAS_{SRP}$ (%)	9	8	6	5	9
$PBIAS_{TP}$	4	1	5	4	3

(%)					
Sample count, SRP	134	157	153	147	90
Sample count, TP	121	138	177	171	107

3.2.3 Estimation of nutrient scaling factors based on reservoir water budgets

One of the goals of my thesis is to estimate time varying TP and SRP retention rates in the reservoir. To do that appropriately, it is important to correctly estimate time varying water fluxes in reservoir inflow and outflow. We used flow information from stream gages at the reservoir inlet and outlet, as well as measured reservoir volume over time to first do a water balance analysis for the Belwood and Conestogo Reservoirs (**Figures 3 and 4**). The water balance equation for a reservoir equates the changes in reservoir volume to the difference in inflows and outflows:

(2) $$\frac{dV(t)}{dt} = Q_{in}(t) + P(t) - Q_{out}(t) - ET(t) + R(t)$$

where

$V(t)$ is the average reservoir volume of month t, in m^3

$Q_{in}(t)$ is the inflow for month t, in m^3

$Q_{out}(t)$ is the outflow for month t, in m^3

$P(t)$ is the direct precipitation for month t on the reservoir surface, in m^3

$ET(t)$ is the evapotranspiration from the reservoir surface, in m^3

$R(t)$ is the non-riverine flux into the reservoir through surface and/or groundwater pathways, in m^3

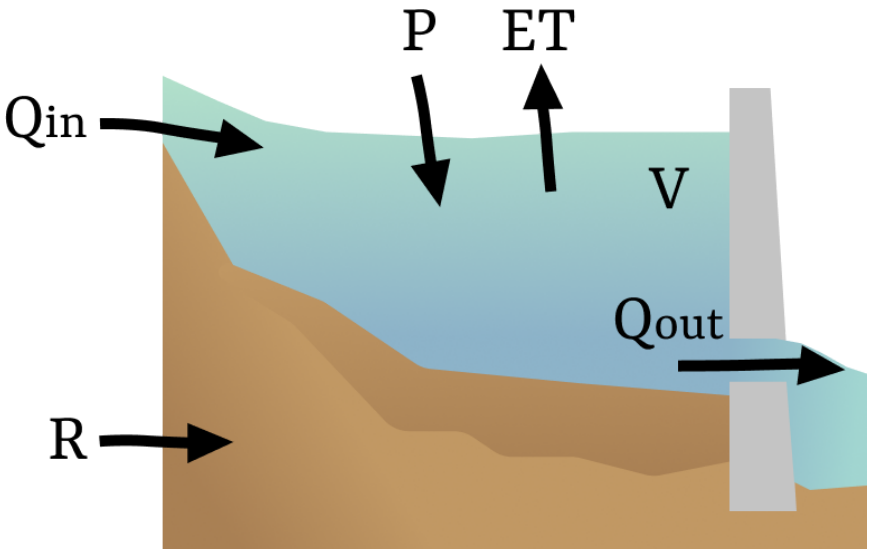

Figure 3. Inflow and outflow terms used in the calculation of the water balance for Belwood and Conestogo Reservoirs.

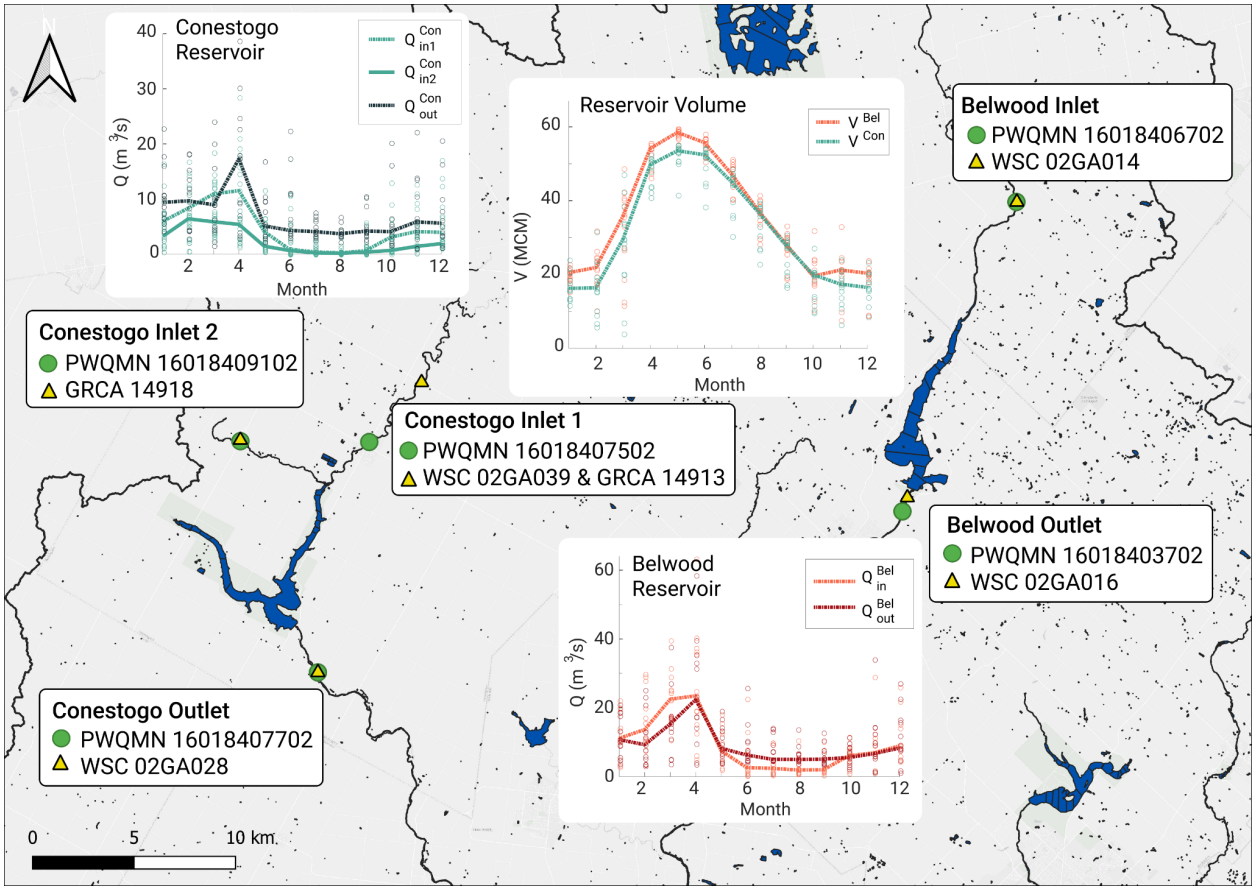

Figure 4. Belwood and Conestogo Reservoirs' water quality and co-located streamflow station IDs and locations, denoted by green dots and yellow triangles respectively. Measured inflow, outflow, and reservoir volume regimes between 2007-2019. Dotted line is monthly median and data points are individual years.

To estimate $R(t)$, I used the measured daily reservoir volumes and the riverine inflows and outflows ($Q_{in}(t)$ and $Q_{out}(t)$) (Section 3.2.1 Data Sources, **Table 1**). This flux is assumed to have the same concentration as $Q_{in}(t)$. Daily precipitation volumes ($P(t)$) were calculated as the product of the maximum reservoir surface area and measured precipitation (in mm) from a nearby climate station (see **Table 1**). Evapotranspiration (in mm) was estimated using the empirical Hargreaves and Samani method (Hargreaves and Samani 1985). The Hargreaves and Samani method requires latitude and measured daily maximum, minimum and mean water temperature data to estimate evapotranspiration (in mm). Since reservoir mean water temperature data was not available, it was estimated as 1.5℃ in the winter (Magee et al. 2016) and inferred from measured air temperature otherwise (Mccombie 1959). Evapotranspiration volume ($ET(t)$)

was then calculated as the product of evapotranspiration rate (in mm) and the maximum surface area of the reservoir. Finally, the groundwater discharge and any surface flow from surrounding area are incorporated into Q_{in}. Then, by equating the terms in **Eq 2**, we can verify the flux data.

However, when equating the change in measured volume to the measured fluxes in **Eq 2**, we discovered an inconsistency since the right hand side did not equal the left hand side. This inconsistency likely appeared because there is uncertainty in discharge measurements and stage-discharge relationships or there is unquantified groundwater or surface water contribution. The $R(t)$ term is used to correct for errors, calculated by rearranging Eq 2:

$$R(t) = \frac{dV(t)}{dt} - Q_{in}(t) - P(t) + Q_{out}(t) + ET(t) \quad (3)$$

Then, a monthly scaling factor (dimensionless) was calculated as:

$$k_{scale,\,month}[-] = \frac{Q_{in,\,month}[L^3] + R_{month}[L^3]}{Q_{in,\,month,\,measured}[L^3]} \quad (4)$$

3.2.4 Metrics estimated

The monthly scaling factor was used when calculating the monthly loads of SRP and TP. Daily load (product of daily concentration and daily discharge) was aggregated to the monthly scale and then multiplied by each month's scaling factor. For example, monthly TP (similarly for SRP) load was calculated as:

$$L_{TP,\,month}[M] = k_{scale,\,month}[-] \bullet \sum_{i=1}^{days}\left(C_{TP}(i)\,[M/L^3] \cdot Q(i)\,[L^3]\right) \quad (5)$$

where $C_{TP}(i)$ [M/L^3] is daily TP concentration modeled by WRTDS

$Q(i)$ [L^3] is total daily discharge

$days$ is the number of days in that month

Similarly, annual TP load was calculated for water years as:

$$L_{TP,\,water\,year}[M] = \sum_{month=3}^{11} L_{TP,\,month}[M] \quad \text{for the months in that water year} \quad (6)$$

Flow-weighted annual concentrations of SRP and TP were calculated for water years as:

(7) $$L_{TP,\,water\ year}\,[M/L^3] \;=\; \frac{\sum_{month=3}^{11} L_{TP,\,month}\,[M]}{\sum_{month=3}^{11} Q_{month}\,[L^3]}$$ for the months in that water year

where $L_{TP,\,month}$ [M] was calculated from Eq 5

$days$ is the number of days in that month

Percent annual retention was calculated for water years as:

(8)

$$TP_{\%\,retained,\,water\ year} = \frac{\sum_{month=3}^{11}\left[k_{scale,\,out,\,month} \bullet \sum_{i=1}^{days} L_{TPin}(i) - k_{scale,\,out,\ month} \bullet \sum_{i=1}^{days} L_{TPout}(i)\right]}{L_{TPin,\,water\ year}}$$

where

$L_{TPin}(i)$ and $L_{TPout}(i)$ [M] are the daily loads of TP into and out of the reservoir,

scaling factor $k_{scale,\,month}$ is unity at the outlet of Belwood, and

summation is over the non-winter months in the water year

SRP:TP was calculated at the inlet and outlet at the monthly scale as:

(9) $$SRP{:}\,TP_{month} = \frac{L_{SRP,\,month}}{L_{TP,\,month}}$$

Similar to the monthly scale, SRP:TP at the annual scale is calculated as the total SRP load that water year over the total TP load that water year:

(10) $$SRP{:}\,TP_{water\ year} = \frac{L_{SRP,\,water\ year}}{L_{TP,\,water\ year}}$$

SRP:TP magnification is defined as the SRP:TP at the outlet over the SRP:TP at the inlet:

(11) $$SRP{:}\,TP\ magnification = \frac{(SRP{:}TP)_{out}}{(SRP{:}TP)_{in}}$$

The error metric used in model calibration is the Nash-Sutcliffe efficiency (Nash and Sutcliffe 1970):

$$NSE = 1 - \frac{\sum_{t=1}^{T} (Q_o^t - Q_m^t)^2}{\sum_{t=1}^{T} (Q_o^t - \overline{Q_o})^2} \quad (12)$$

where $\overline{Q_o}$ is the mean of observed values, Q_m^t is the modeled value and Q_o^t is the observed value at time t.

In this thesis, the seasons are defined as follows: winter is December - February, spring is March - May, summer is June - August, and fall is September - November.

3.2.5 Uncertainty and sensitivity analysis

The uncertainty associated with using the WRTDS model was estimated using the EGRETci package which uses WRTDSKalman. Confidence intervals around the flux for each month were obtained. Using the monthly confidence intervals, the error bounds around the percent SRP and TP retention were calculated using basic rules of propagation of error.

To evaluate the sensitivity of each model parameter, a one-at-a-time (OAT) sensitivity analysis was conducted. Each model parameter was perturbed by 10% and the resultant percent change was reported.

3.3 Model Development

Research Objective 2 was to model P speciation over time and sediment P accumulation. Here I describe how I built this model, from inception to calibrated results.

3.3.1 Model schematic and the system of differential equations governing the model

I developed a P cycling model based on measured streamflow and concentrations to study the seasonal P dynamics within reservoirs. The 9-box biogeochemical model assumes that Belwood Reservoir is a continuous stirred-tank reactor and simulates the cycling and speciation of P at the monthly scale. The model created here incorporates sediment P pools in order to capture internal loading dynamics. A mass balance modeling approach (**Figure 5**) was used to represent the key biogeochemical processes controlling P cycling in reservoirs. The benefit of

separating P species in the model is that it enables us to investigate the processes acting to retain and release SRP and particulate P, and allows us to study the change in SRP:TP seasonally and annually.

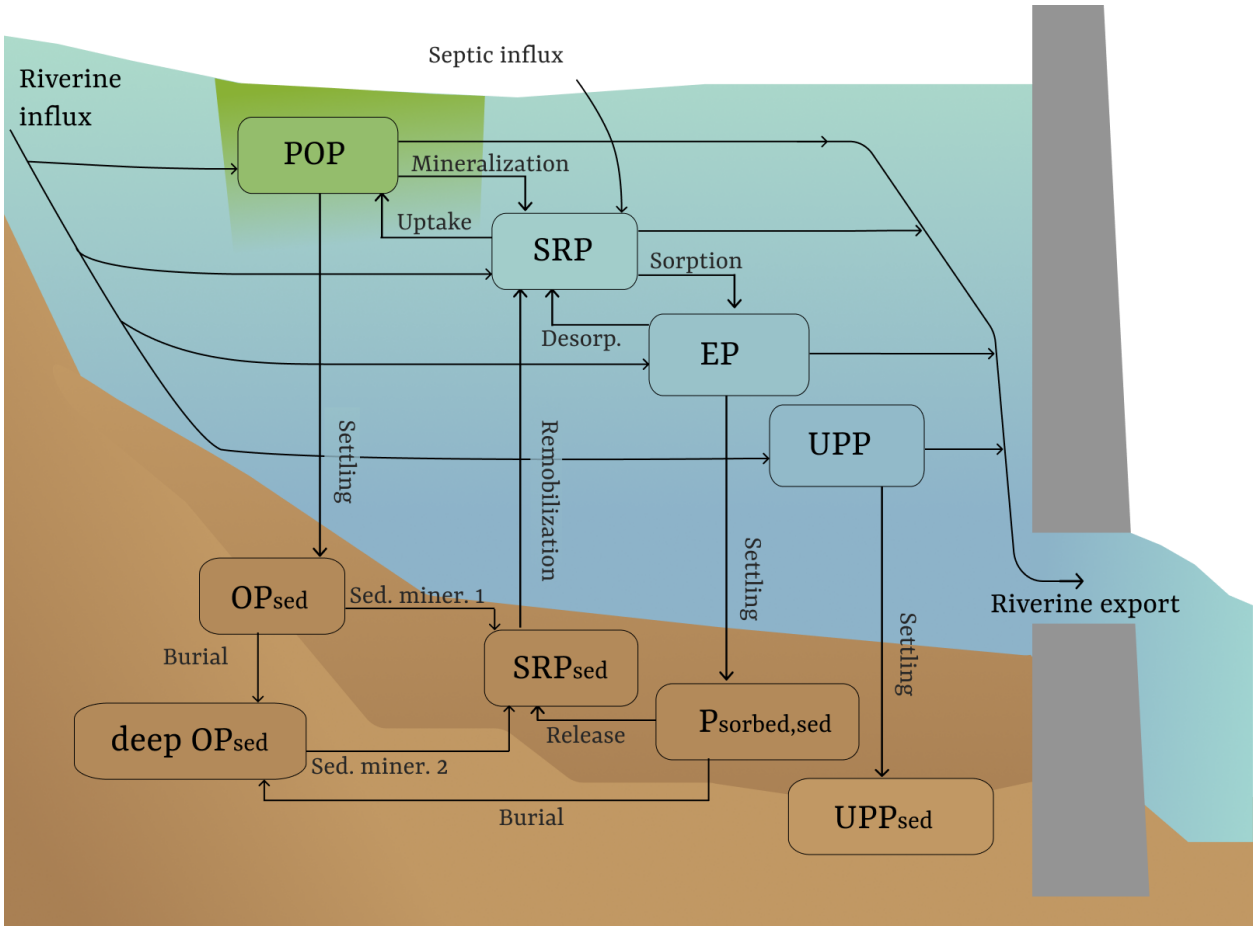

Figure 5. The mass balance schematic used to simulate cycling and retention of P in reservoirs. The nine pools modeled (described in Table 3) are SRP, POP, EP and UPP in the water column, and OP_{sed}, SRP_{sed}, $P_{sorbed,\ sed}$, UPP_{sed}, and deep OP_{sed} in the sediment. The arrows represent the processes transforming P.

The model developed here separates P in the water column and sediment into four pools (described further in **Table 3**): soluble reactive P (SRP), particulate organic P (POP), exchangeable P (EP), and unreactive particulate P (UPP) in the water-column, and sediment porewater SRP (SRP_{sed}), sediment organic P (OP_{sed}), sorbed sediment P ($P_{sorbed,\ sed}$), deep sediment organic P (deep OP_{sed}) and sediment unreactive particulate P (UPP_{sed}).

Table 3. State variables simulated by the model

State Variable	Description	Processes Undergone
SRP	Soluble reactive phosphorus in the water column. SRP is the pool of bioavailable P (Rigler 1964) and consists mostly of inorganic, dissolved P.	Sorption to oxides, clay minerals and organic matter, uptake by phytoplankton for primary production
POP	Particulate organic phosphorus in the water column. POP includes P contained in organisms and detrital organic molecules (Labry et al. 2013).	Mineralization/phytoplankton mortality, sedimentation to OP_{sed}
EP	Exchangeable phosphorus in the water column. EP is considered the P molecules that exchange with clay minerals, oxides and organic matter, such as orthophosphate and organic P (Maavara et al. 2015).	Sedimentation to $P_{sorbed, sed}$, desorption from oxides, clay minerals, and organic matter
UPP	Unreactive particulate phosphorus in the water column. UPP is crystalline phosphate minerals that are considered inert within relevant timescales (Maavara et al. 2015).	Sedimentation to UPP_{sed}
SRP_{sed}	Porewater SRP in lake sediment	Remobilizes to water column SRP
OP_{sed}	Organic P in lake sediment	Mineralizes to pore water SRP
Deep OP_{sed}	Organic P stored in deep lake sediments	Slowly mineralizes to pore water SRP
$P_{sorbed, sed}$	P sorbed to clay and iron, in lake sediment	Desorbs to pore water SRP
UPP_{sed}	Unreactive particulate P in lake sediment	Comes from sedimenting UPP in the water column and becomes permanently unavailable in the lake sediment

In order to model these P pools over time, a system of differential equations was derived to capture the mass fluxes between P pools, driven by biogeochemical processes. The differential equations that form the basis of the model are as follows:

(13) $$\frac{d\,SRP}{dt} = SRP_{in} + SRP_{septic} + k_{miner} \cdot POP + k_{desorp} \cdot EP - k_{up} \cdot SRP - k_{sorp} \cdot SRP + k_{remob,\,seas} \cdot SRP_{sed} - \frac{SRP}{V} \cdot Q_{out}$$

(14) $$\frac{d\,POP}{dt} = \frac{\alpha_{POP}}{\alpha_{PP}} \cdot PP_{in} + k_{up} \cdot SRP - k_{miner} \cdot POP - k_{POPsett,\,seas} \cdot POP - p_{prop,\,exp} \cdot \frac{POP}{V} \cdot Q_{out}$$

(15) $$\frac{d\,EP}{dt} = \frac{\alpha_{EP}}{\alpha_{PP}} \cdot PP_{in} + k_{sorp} \cdot SRP - k_{desorp} \cdot EP - k_{sett} \cdot EP - \frac{EP}{V} \cdot Q_{out}$$

(16) $$\frac{d\,UPP}{dt} = \frac{\alpha_{UPP}}{\alpha_{PP}} \cdot PP_{in} - k_{sett} \cdot UPP - \frac{UPP}{V} \cdot Q_{out}$$

(17) $$\frac{dSRP_{sed}}{dt} = k_{miner1,\,sed} \cdot OP_{sed} + k_{miner2,\,sed} \cdot deep\,OP_{sed} - k_{remob,\,seas} \cdot SRP_{sed} + k_{release,\,sed,\,seas} \cdot P_{sorbed,\,sed}$$

(18) $$\frac{dOP_{sed}}{dt} = k_{POPsett,\,seas} \cdot POP - k_{miner1,\,sed} \cdot OP_{sed} - k_{bur} \cdot OP_{sed}$$

(19) $$\frac{dP_{sorbed,\,sed}}{dt} = k_{sett} \cdot EP - k_{release,\,sed,\,seas} \cdot P_{sorbed,\,sed} - k_{bur} \cdot P_{sorbed,\,sed}$$

(20) $$\frac{dUPP_{sed}}{dt} = k_{sett} \cdot UPP$$

(21) $$\frac{d\,deep\,OP_{sed}}{dt} = k_{bur} \cdot OP_{sed} + k_{bur} \cdot P_{sorbed,\,sed} - k_{miner2,\,sed} \cdot deep\,OP_{sed}$$

Where:

$f = (SRP, POP, EP, UPP, SRP_{sed}, OP_{sed}, P_{sorbed,sed}, UPP_{sed}, deep\,OP_{sed})$ [M] are state variables described in **Table 3**

SRP_{in} and $PP_{in} = TP_{in} - SRP_{in}$ [MT^{-1}] are the time-varying external loading to the reservoir

Q_{out} [L^{3}T^{-1}] is the time-varying discharge out of the reservoir

V [L^3] is the time-varying volume of the reservoir

$\alpha_{PP} = \alpha_{POP} + \alpha_{EP} + \alpha_{UPP}$, $where\ \alpha_{POP} = 0.04,\ \alpha_{EP} = 0.15,\ \alpha_{UPP} = 0.72$ [-] are constants of riverine influx proportions for POP, EP and UPP, estimated as the global average (Meybeck 1993, Compton et al. 2000, Maavara et al. 2015)

k [T^{-1}] are model parameters described below and in **Table 4**

$p_{prop,exp}$ is the proportion of POP that may exit the reservoir via flow

$k_{release,sed,seas}$ is a calibrated parameter for the summer and is equal to 1 otherwise

$k_{POPsett,seas}$ and $k_{remob,seas}$ are seasonally calibrated (winter, spring, summer, fall)

$k_{up} = \mu'(T)\frac{SRP}{P'_D + SRP}$ describes phosphate and temperature dependence of P uptake in the water column (Saloranta and Andersen 2007), assuming no light limitation, where:

$\mu'(T) = \mu 20 \cdot \theta^{T-20}$ [T^{-1}] describes temperature dependence of P uptake

$\mu 20$ [T^{-1}] is a parameter for the uptake rate at reference temperature (20℃)

P'_D [ML^{-3}] is the half-saturation parameter

T [K] is the water temperature, inferred from air temperature (using (Mccombie 1959, Magee et al. 2016))

$\theta = exp(10^{-1} \cdot ln\,2)$ [-] since we assume that biological rates double on a 10℃ temperature increase (Saloranta and Andersen 2007)

$k_{miner} = m20 \cdot \theta^{T-20}$ describes mineralization in water column (Saloranta and Andersen 2007), where:

$m20$ [T^{-1}] is a parameter for the mineralization rate of P in the water column at a reference temperature (20℃)

T and θ are the same as above

$k_{miner1,\,sed} = m20_{sed,1} \cdot \theta^{T-20}$ and $k_{miner2,\,sed} = m20_{sed,2} \cdot \theta^{T-20}$ describe two mineralization rates in the sediment (Saloranta and Andersen 2007), where:

$m20_{sed,1}$ and $m20_{sed,2}$ are two parameters for the fast and slow mineralization rates of P in the sediment at a reference temperature (20℃), respectively

T and θ are the same as above.

The differential equations govern the relationship between state variables, input time series vectors, and model parameters. All fluxes are assumed to follow first-order rate equations (see **Eqs. 13-21**). For example, the flux from SRP to POP is expressed as $k_{up} \cdot SRP$ where k_{up} is the uptake rate parameter [T^{-1}] and SRP is the mass of SRP in the reservoir in a particular month [M]. A solution f to the system of equations is a set of time series, one for each of the state variables that were described above.

To get a solution, certain input time series are required by the model. The input time series are riverine SRP flux (SRP_{in}), riverine TP flux (TP_{in}), reservoir volume (V), and reservoir dam discharge (Q_{out}). The input fluxes of SRP and TP were calculated as the product of measured riverine concentration and measured streamflow. The particulate P (calculated as inlet TP load minus inlet SRP load) was proportioned into POP, EP, and UPP using global average riverine proportions (Meybeck 1993, Compton et al. 2000, Maavara et al. 2015).

Model parameters, described in **Table 4**, which are associated with relevant biogeochemical processes and the estimated fluxes between P pools. The range of values that the model parameters could take were bounded by values reported in the existing literature (**Table 4**), and were calibrated to the measured SRP and TP export loads. Finally, the system of differential equations (**Eqs. 13-21**) was solved using the robust fourth-order numerical method, Runge-Kutta (RK4). A time step of $h = 0.001\,year$ was used to ensure stability. The model was coded in Matlab 2018b and the RK4 implementation is included in the Appendix.

The initial conditions were set based on measured averages when possible. That is, the SRP and TP mass in the reservoir were estimated using the average measured SRP and TP concentrations at the outlet. Since measurements of POP, EP and UPP were not available, global riverine averages (α constants) were used to proportion the particulate P in the water column. For the partitioning of particulate P in the sediment, global riverine averages were used again. To remove the effect of initial conditions, the model was run for a spin up period of five years. Model inputs during the spin up period were the same as inputs from the first year (2007), effectively running 2007 for six years in a row. The spin up period allowed the model to stabilize to a state of system equilibrium.

Table 4. Model parameters

Parameter	Value	Description	References
k_{sorp}	0.01-0.1250 $month^{-1}$	Rate coefficient of sorption of dissolved P to exchangeable P	Gorham and Boyce 1989, Katsev et al. 2006, Maavara et al. 2015
k_{desorp}	0.00083-0.1667 $month^{-1}$	Rate coefficient of desorption of P from organic matter to dissolved form	Gorham and Boyce 1989, Maavara et al. 2015
$p_{prop,exp}$	0-1 (-)	Proportion of POP pool that is allowed to exit the reservoir via riverine outflow	Calibrated parameter
m20	0.1-0.3 (day^{-1})	Water column mineralization rate of POP in a reference temperature of 20°C	Saloranta and Andersen 2007
μ20	1.0-1.5 (day^{-1})	Water column uptake rate of SRP in a reference temperature of 20°C	Saloranta and Andersen 2007
P'_D	0.2-2 (mg m^{-3})	Half-saturation parameter for uptake	Saloranta and Andersen 2007
$k_{remob,seas}$	0-10 $month^{-1}$	Rate coefficient of remobilization of P from sediment. Four parameters: one for each season	Calibrated parameters
k_{sett}	0.1680-24 $month^{-1}$	Rate coefficient of EP and UPP settling from water column to sediment	Bolin et al 1987, Grimard & Jones 1982
$k_{POPsett,seas}$	0-10 $month^{-1}$	Rate coefficient of sedimentation of POP in water column to OPsed. Four parameters: one for each season	Calibrated parameters
$m20_{sed,1}$	0.1-0.3 (-)	Sediment mineralization rate of OP_{sed} in a reference temperature of 20°C	Saloranta and Andersen 2007
$m20_{sed,2}$	0-0.0001 (-)	Sediment mineralization rate from deep OP_{sed} pool in a reference temperature of 20°C	Calibrated parameter
k_{bur}	0-10 $month^{-1}$	Burial of OPsed and EPsed to deep OPsed pool	Calibrated parameter
$k_{release,sed,seas}$	0.00083-0.1667 $month^{-1}$	Rate coefficient of desorption of P from organic matter to dissolved form in the sediment. Two parameters: one for the summer and one for the other seasons	Gorham and Boyce 1989, Maavara et al. 2015

3.3.2 Model parameter sensitivity analysis

To assess the sensitivity of each model parameter, I conducted a one-at-a-time (OAT) sensitivity analysis. Each parameter value was perturbed by ±10% from the base parameter set.

The parameter set used for the base case was the set with the best NSE for SRP and TP export. **Table 5** summarizes the resultant percent change (Δpbias) of monthly SRP export, TP export, and SRP:TP magnification. Percent changes greater than 1% are bolded. The most sensitive parameters were $m20$ (associated with mineralization rate), $\mu 20$ (associated with uptake rate), settling rates of POP, and the slow mineralization rate from deep OP_{sed} to OP_{sed}.

Table 5. Model parameter sensitivity results

Model parameter	Base case value	$\Delta pbias_{SRPout}$ with 10% increase (10% decrease reported in brackets) (%)	$\Delta pbias_{TPout}$ with 10% increase (10% decrease reported in brackets) (%)	$\Delta pbias_{mag}$ with 10% increase (10% decrease reported in brackets) (%)
k_{sorp}	0.0150	0.018 (0.018)	0.022 (0.022)	0.005 (0.005)
k_{desorp}	0.1448	0.002 (0.002)	0.003 (0.003)	4e-4 (4e-4)
$p_{prop,exp}$	0.4739	**1.39 (1.45)**	0.81 (0.84)	0.27 (0.28)
m20	0.2774	0.64 (0.65)	**3.54 (3.61)**	**2.93 (3.04)**
$\mu 20$	1.0203	**1.40 (1.66)**	**7.15 (8.40)**	**5.68 (6.45)**
P'_D	0.6315	0.03 (0.03)	0.15 (0.15)	0.12 (0.12)
$k_{remob,\ wint}$	0.5621	0.56 (0.61)	0.21 (0.23)	0.09 (0.10)
$k_{remob,\ spr}$	5.7433	0.18 (0.22)	0.14 (0.22)	0.01 (0.01)
$k_{remob,\ summ}$	8.7791	0.01 (0.01)	0.002 (0.003)	0.008 (0.010)
$k_{remob,\ fall}$	2.9298	0.18 (0.22)	0.27 (0.32)	0.004 (0.004)
k_{sett}	12.4040	0.25 (0.29)	7e-5 (8e-5)	0.16 (0.19)
$k_{POPsett,\ wint}$	7.5865	0.54 (0.64)	0.24 (0.29)	0.63 (0.68)
$k_{POPsett,\ spr}$	1.0125	**1.55 (1.68)**	0.76 (0.82)	0.31 (0.31)
$k_{POPsett,\ summ}$	2.8793	**1.33 (1.55)**	0.75 (0.88)	0.88 (0.90)
$k_{POPsett,\ fall}$	5.9055	**1.04 (1.24)**	0.58 (0.69)	**1.24** (0.92)
$m20_{sed,1}$	0.0265	0.25 (0.25)	0.25 (0.25)	0.003 (0.003)
$m20_{sed,2}$	8.3303e-5	**9.02 (8.07)**	**9.12 (8.15)**	0.07 (0.07)

k_{bur}	7.6235	0.23 (0.28)	0.23 (0.28)	0.003 (0.004)
$k_{release,sed,summ}$	0.1413	4e-4 (4e-4)	3e-4 (3e-4)	6e-7 (6e-7)
$k_{release,sed,other}$	0.1505	0.001 (0.001)	0.002 (0.002)	3e-5 (3e-5)

4.0 Results and Discussion

4.1 Reservoirs on seasonal and annual P speciation: data analysis

For Research Objective 1, I have analyzed reservoirs' role in P speciation in two local, multi-purpose reservoirs that have seen annual algal blooms in recent years, Belwood and Conestogo Reservoirs. Here, I present an overview of annual reservoir TP retention over time, and SRP and TP concentrations over time at the inlet and outlet of both reservoirs. Next, I analyze the ratio of SRP:TP over time at the inlet and outlet to investigate the impact of reservoirs on SRP:TP. Finally, I analyze how each of these relationships vary seasonally. A better understanding of the seasonality of SRP and TP in these reservoirs will help us to identify best management practices to mitigate algal blooms in the reservoirs and support the health of downstream ecosystems, including Lake Erie.

4.1.1 Reservoirs alter watershed P dynamics: Annual Scale Effects

I found the annual flow-weighted concentrations (**Eq 7**) of TP to be lower at the outlet compared to the inlet for Belwood Reservoir in 8 of the 12 years studied (**Figure 6a**) and the same was found for SRP flow-weighted concentrations (**Figure 6c**), however the years did not coincide exactly. At Conestogo Reservoir, annual flow-weighted TP concentrations at the inlet and outlet were very close (**Figure 6b**), with similar results observed for SRP (**Figure 6d**).

The sink/source behaviour of both reservoirs is quantified by the annual percent retention (**Figure 6e and 6f**), as defined in **Eq 8**, where a positive percent retention reflects sink behaviour and a negative percent retention reflects source behaviour. Annual percent retention is calculated for each water year excluding winter months (December - February) because of the sparsity of winter concentration data. The percent TP retention for Conestogo Reservoir varies between -72% in 2016 to 25% in 2008, while percent TP retention in Belwood Reservoir is generally

higher, from -40% in 2019 to 32% in 2017 (**Figure 6e**). These numbers are similar to a study that found TP retention was 26 ± 31% (mean ± SD) for 17 reservoirs across the US (Powers et al. 2015). Error bounds have been included around the estimates of SRP and TP retention. The uncertainty is calculated using the confidence intervals from using WRTDSKalman which is detailed in Section 3.2.5.

Both the Belwood and Conestogo Reservoirs fluctuate between being a source and a sink for SRP (**Figure 6f**). The SRP retention in Belwood Reservoir varied from -68% in 2009 to 43% in 2017, while SRP retention in Conestogo Reservoir varied between -71% in 2011 and 28% in 2008. Interestingly, the source-sink behaviour is visible for both SRP and TP and they are similar between years. For example, in years that Belwood Reservoir acts as a source of TP, the reservoir often acts as a source of SRP too.

Interestingly, the annual ratio of SRP:TP at the outlet is greater than the inlet for Belwood Reservoir in most years (7 out of 12 years) (**Figure 6g**), indicating that the reservoir contributes to a magnification of the bioavailable P fraction. In contrast, Conestogo Reservoir fluctuates in behaviour (**Figure 6h**). This magnification effect at Belwood Reservoir has important consequences for downstream waters where an increase in the bioavailable P fraction is often related to an increase in algal blooms (Watson et al. 2016).

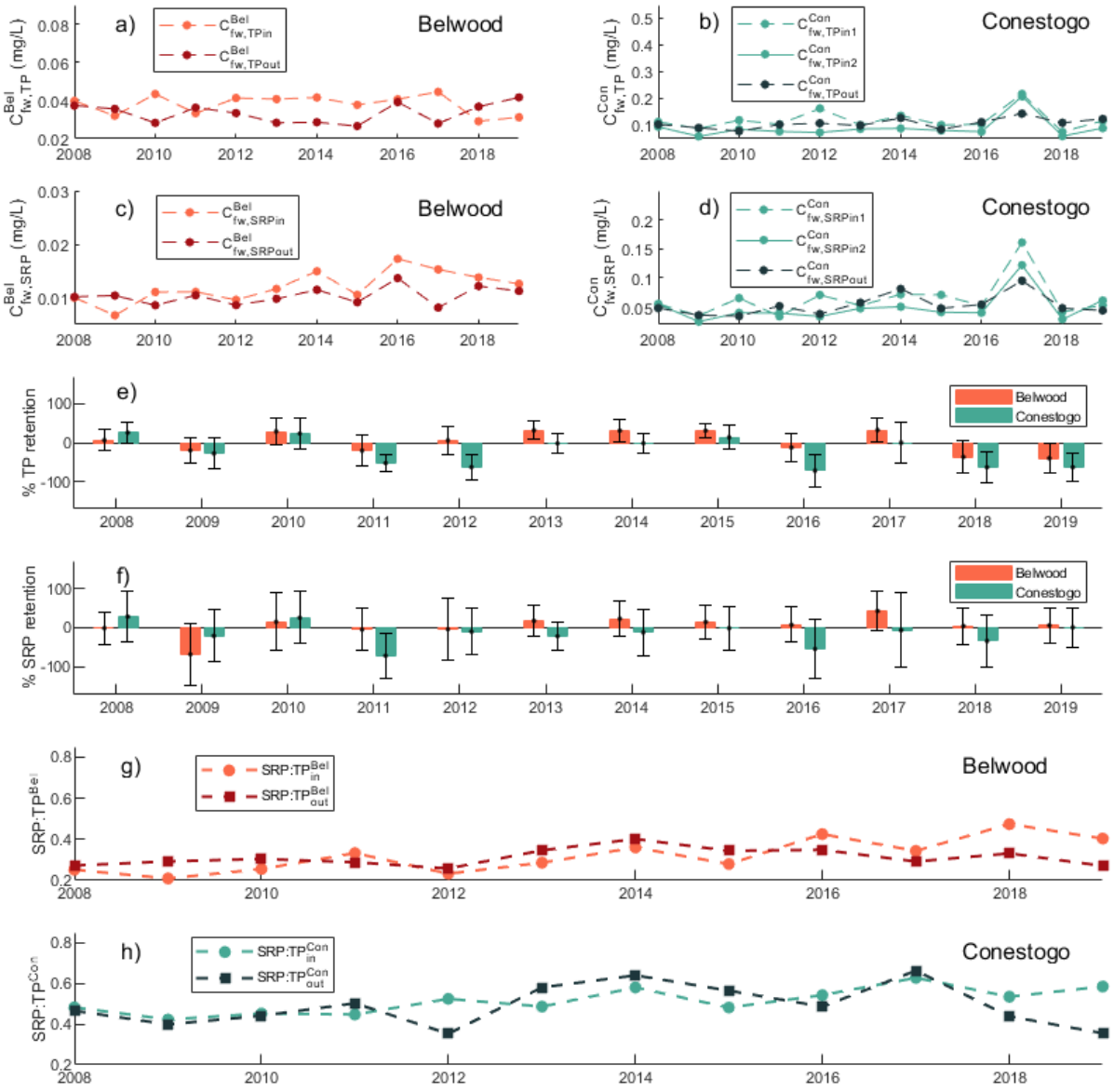

Figure 6. Annual flow-weighted TP (a and b) and SRP (c and d) concentrations at the inlets (lighter shades) and outlets (darker shades) of Belwood and Conestogo Reservoir between 2007-2019. Annual percent of TP (e) and SRP (f) retained by the reservoirs. Annual estimates of SRP:TP at the inlet and outlet of Belwood (g) and Conestogo (h). All annual values were estimated using water years and excluding winter months (Dec-Feb) since these months were unreliable.

4.1.2 Seasonality of SRP and TP concentrations and loads

In Section 4.1.1, I showed that Belwood and Conestogo Reservoirs were fluctuating between a source and a sink for SRP and TP at the annual scale between 2008-2019. At the sub-annual scale, reservoirs can act as sources or sinks depending on season (Powers et al. 2015, Shaughnessy et al. 2019). To determine the seasonal source vs sink behaviour in Belwood and Conestogo Reservoirs, we looked at monthly total loads (**Eq 5**) at the inlets and the outlets. If the P load into the reservoir is greater than the load out in a month, then the reservoir is acting as a sink that month. Conversely, if the load out of the reservoir is greater than the influx in a month, the reservoir is acting as a P source that month. The winter months are omitted throughout because of the sparsity of measured data during those months, and thus conclusions about source/sink behaviour in the winter cannot be drawn.

The seasonal regimes of median concentrations (C_{SRP} and C_{TP}; column 1) and discharge (column 2) are included in **Figure 7** to understand the loading regimes (L_{SRP} and L_{TP}; column 3) at Belwood and Conestogo Reservoirs. P loading regimes reveal that Belwood Reservoir acts as a sink for TP in March - May then transitions to a source for June - October (**Figure 7c**). At Conestogo Reservoir, TP load regimes suggest sink behaviour for March, then transitions to a source for April - October (**Figure 7f**). The source behavior at both reservoirs in the summer and fall is attributed to a combination of: higher TP concentrations at the outlet compared to the inlet (**Figure 7a and 7d**), and higher outlet flows compared to inlet flows in the warmer months (**Figure 7b and 7e**).

Belwood Reservoir acts as a sink for SRP in March then acts approximately net neutral in April and May, before turning to a source for SRP through the summer (June - September) (**Figure 7i**). The Conestogo Reservoir acts as a sink for SRP during March and then transitions to a source through April - September (**Figure 7ℓ**). Similar to TP, the summer SRP source-behaviour observed in both Conestogo and Belwood Reservoirs is driven by both concentration (**Figure 7g and 7j**) and discharge (**Figure 7h and 7k**). SRP concentrations at the outlet of Belwood Reservoir exhibits a peak in the summer months (**Figure 7g**), likely driven by summer septic loading and redox-related P release from lake sediment (Ekholm et al. 1997, Shaughnessy et al. 2019).

Other notable observations warrant further investigation. It is interesting to note that there is an amplification and shift in C^{Bel}_{TP} peak by two months from inlet to outlet at Belwood Reservoir (**Figure 7a**). This is an interesting demonstration of the P cycling occurring and could be described as particulate P entering the reservoir in the spring, cycling to SRP and organic matter from uptake during the summer, and is released in the form of detritus around September. The elevated SRP and TP concentrations at the outlet in the summer (**Figure 7a and 7g**) could also be a product of the summer septic inputs to Belwood Reservoir from surrounding camps and cottages that are not measured at the riverine inlet.

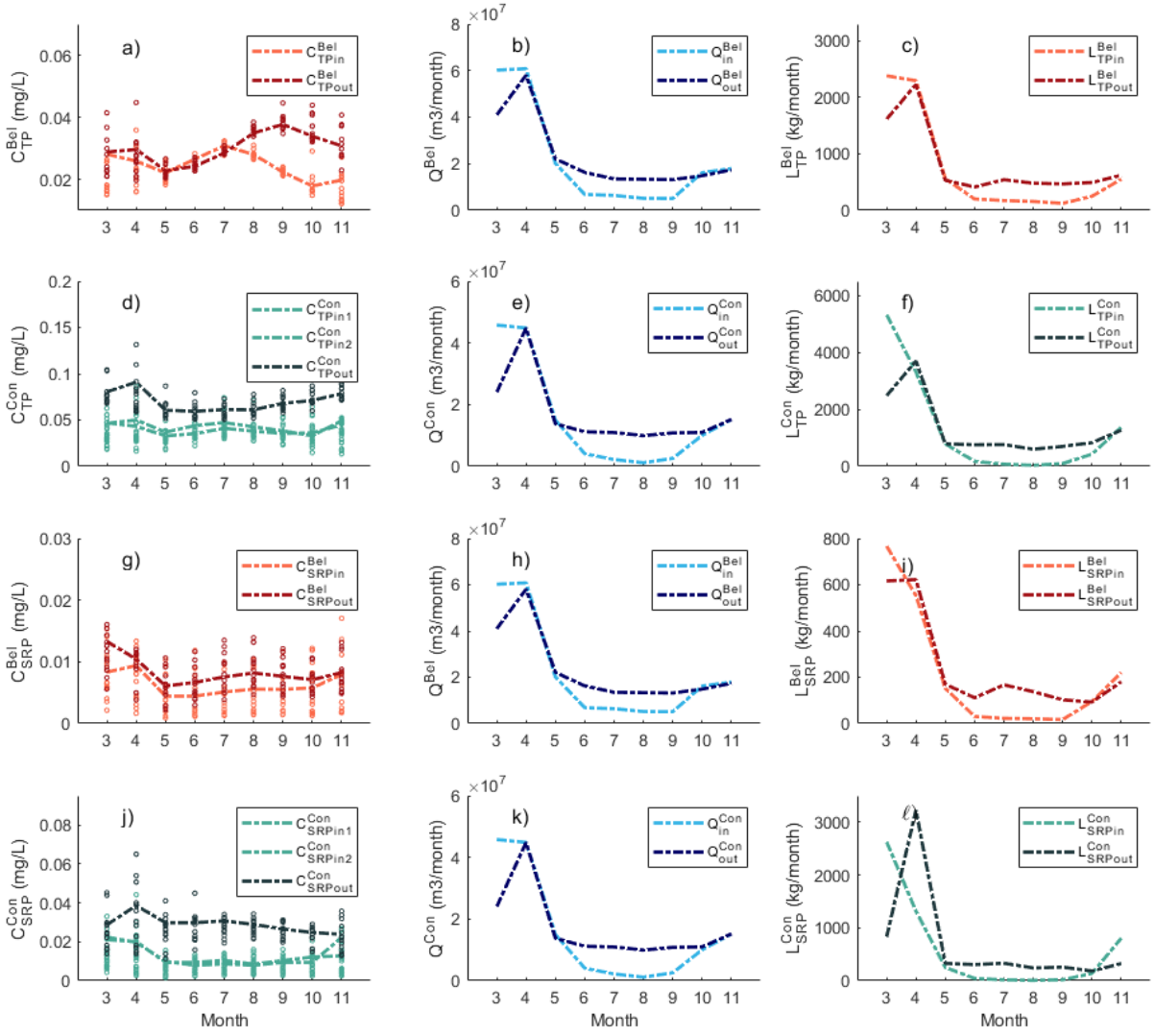

Figure 7. Median concentration (column 1), median discharge (column 2) and median load (column 3) regimes for TP and SRP at Belwood (rows 1 and 3, respectively) and Conestogo (rows 2 and 4, respectively) Reservoirs between 2007-2019. Dashed lines are the median taken over all years and data points are individual years. December to February are omitted because of the sparsity of measured data during those months.

4.1.3 Seasonality of SRP:TP from the inlet to the outlet

To further understand the impact of reservoirs on the seasonal speciation of P, the monthly SRP:TP magnification from inlet to outlet in both reservoirs was examined. I used a ratio of ratios to quantify the magnification of SRP:TP from inlet to outlet (**Eq 11**). When the SRP:TP is greater at the outlet than the inlet, the magnification factor is greater than 1 (**Figure**

8). Notably, in the summer, the SRP:TP is nearly doubled along the stream by both Belwood and Conestogo Reservoirs (**Figure 8a and 8b**). Both reservoirs peak in SRP:TP magnification in the month of July, approximately doubling the SRP:TP along the stream. The summer magnification of the bioavailable P fraction is more significant in Conestogo Reservoir compared to Belwood Reservoir. In Belwood Reservoir in the spring (March - May) and fall (September - November), SRP:TP has a magnification factor around 1, meaning that the outlet ratio is close to the inlet ratio. In Conestogo Reservoir in the spring, the reservoir transitions from a magnification factor around 0.7 to 1.5. In the fall, Conestogo Reservoir transitions from a magnification factor of 1.4 to 0.75.

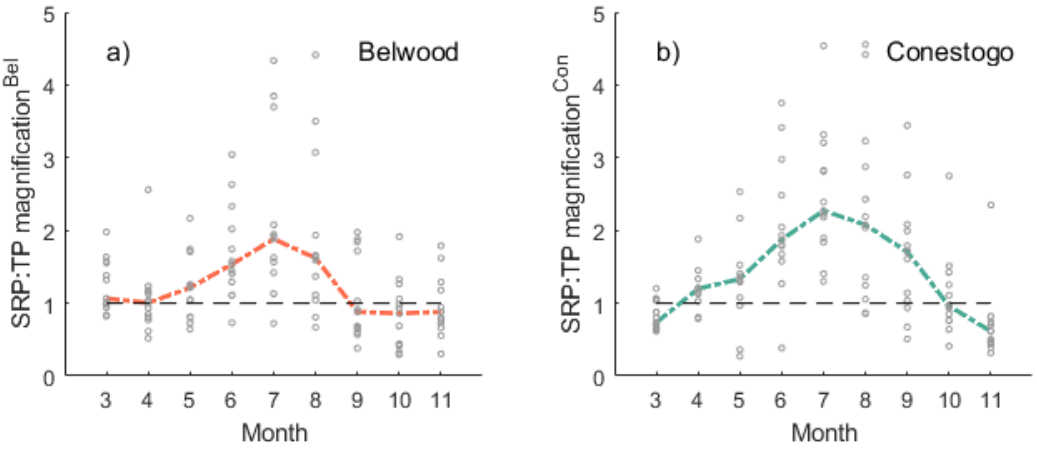

Figure 8. SRP:TP magnification from inlet to outlet at a) Belwood and b) Conestogo Reservoirs. The dashed line is the median between 2007-2019 and each point represents the SRP:TP magnification in a particular year. December to February are omitted because of the sparsity of measured data during those months.

4.2 Modeling P Retention and Release in Belwood Reservoir

Research Objective 2 was to create a model that captures both P speciation over time and legacy P accumulation. First I have included model calibration results and then the modeled seasonal P pools and fluxes.

4.2.1 Parameter set selection and resulting model fit

The model was calibrated using OSTRICH (Matott 2017), a parameter calibration tool. The objective functions used to determine the suitability of a parameter set were: Nash-Sutcliffe Efficiency (NSE), defined in Section 3.2.4 (**Eq 12**), of monthly SRP (NSE_{SRP}) and TP (NSE_{TP}) loads at the reservoir outlet, and NSE of monthly SRP:TP magnification from inlet to outlet (NSE_{mag}). The model was calibrated at the monthly scale between 2007-2019, excluding winter months (December, January and February) due to sparse measured concentrations. OSTRICH was run for 1000 iterations and resulted in 178 nondominated parameter sets. We found 174 parameter sets where NSE_{SRP} ranged from 0.57-0.86, NSE_{TP} from 0.60-0.91, and NSE_{mag} from -4.6-0.22 (**Figure 9**). Thus, the calibrated parameter sets were able to capture SRP and TP export dynamics well. In comparison, SRP:TP magnification was more difficult to calibrate for. Although SRP and TP loads were captured well, a slight variation from the measured values could combine for a more significant variation from measured magnification. This can be seen by the peak in modeled SRP:TP magnification in July 2007.

Parameter set selection plays an important role in model performance. Interestingly, when using the parameter set with the best fit of SRP and TP export (NSE_{SRP} = 0.86 and NSE_{TP} = 0.88) for the full time period (2007-2019), the modeled SRP:TP magnification fits measured data fairly well with NSE_{mag} = 0.53 during the second half of the time period (2013-2019). The overall poor NSE_{mag} range reported above reflects that the model is unable to capture the SRP:TP magnification over the full time period (as shown in **Figure 9c**). It seems as though the modeled SRP:TP magnification in the 2007-2012 period acts very differently than the 2013-2019 period. This modeled behaviour is something that should be investigated in future work.

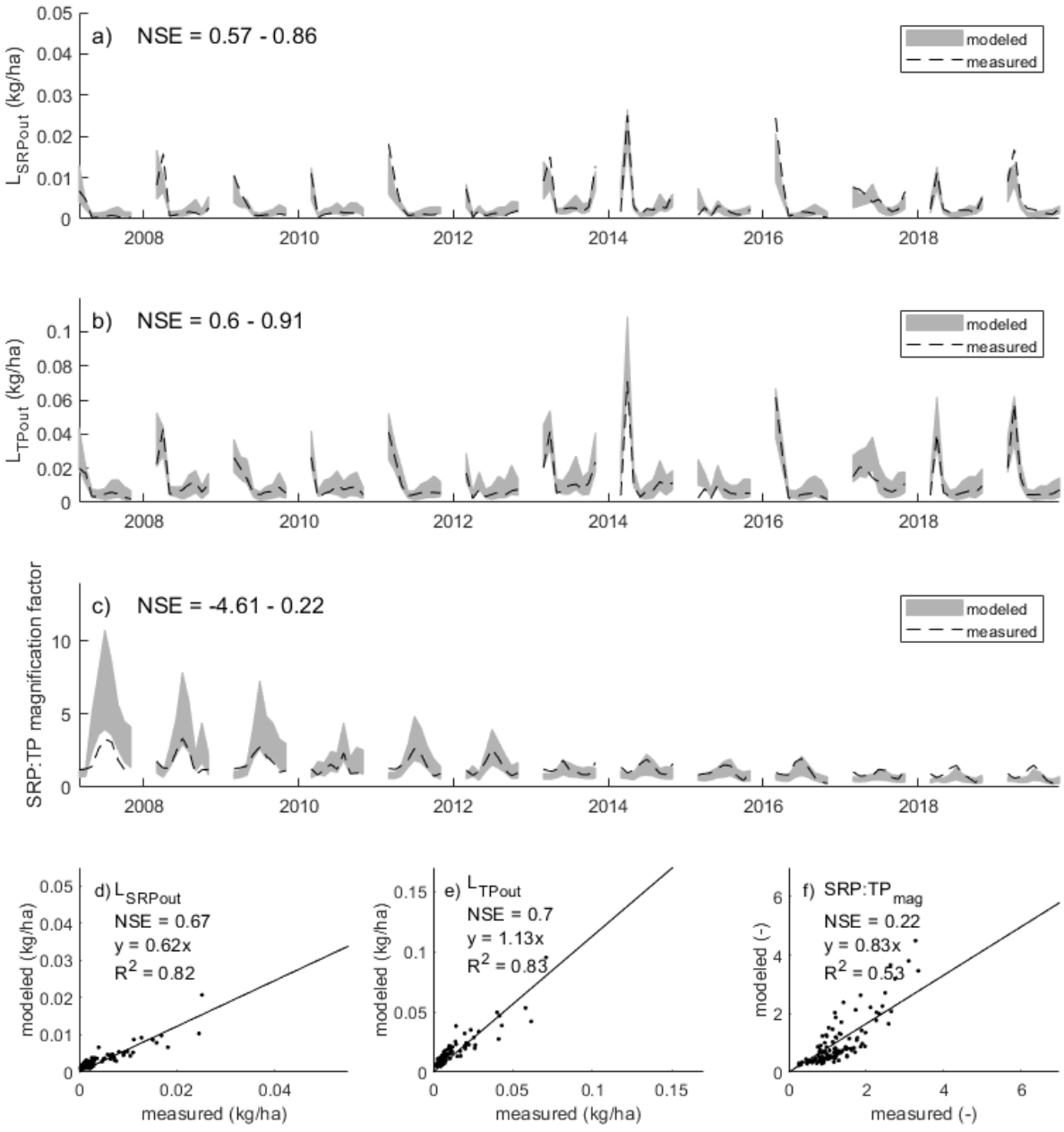

Figure 9. Modeled a) SRP and b) TP export with uncertainty bounds for 2007-2019. Dashed line is the measured monthly load. Uncertainty bounds are the monthly maximum and minimum modeled values of the filtered nondominated parameter sets, so the lower and upper limits don't necessarily exist as a particular time series. d-f) Measured load against modeled load using the parameter set with the highest NSE_{mag} = 0.22.

Although the model does a fair job at capturing SRP and TP export, the monthly SRP:TP magnification was more difficult to model (**Figure 9c and 10c**). When studying one parameter set, the set with best NSE_{SRP} and NSE_{TP} (0.86 and 0.88 respectively), the model is able to capture

the SRP:TP magnification in some months. The modeled SRP:TP magnification through the spring and summer is fairly close to measured magnification, however the fall months were not captured well (**Figure 10c**). During the fall, the poor model estimation is in part because of underprediction of TP export (**Figure 10a**) and overprediction of SRP export (**Figure 10b**). Again, parameter set selection plays an important role in the model performance, especially with respect to SRP:TP magnification.

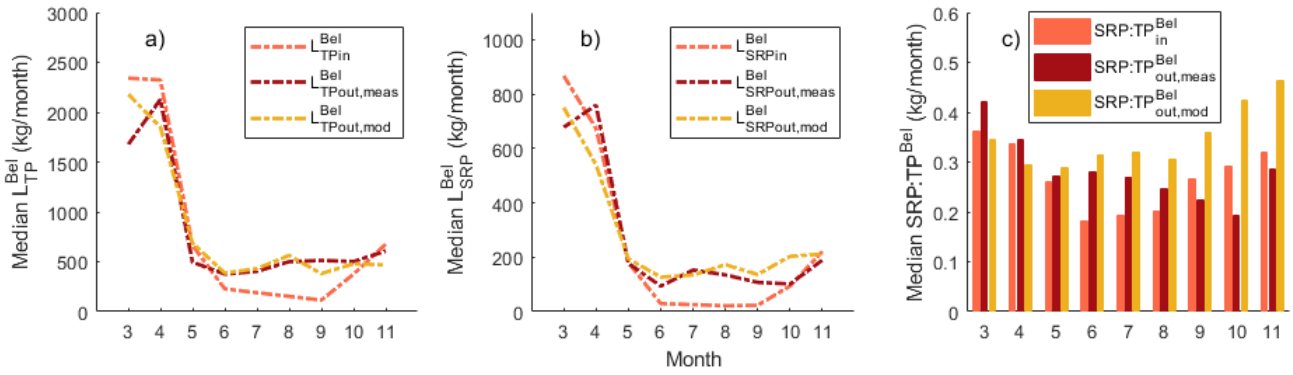

Figure 10. Monthly median a) TP loads, b) SRP loads, and c) SRP:TP ratio at the inlet (measured) and outlet (measured and modeled).

The model was unable to capture the sediment P accumulation in Belwood Reservoir (**Figure 11**). From sediment core data, we expect Belwood Reservoir to accumulate approximately 45 tonnes/year on average. Although the model was generally able to capture the increasing trend of sediment TP, the average modeled accumulation rate was only approximately 6-10 tonnes/year. The accumulation from external inputs can be estimated roughly as the measured influx of TP minus the measured efflux of TP, which is approximately 3-4 tonnes/year on average. Thus the remaining sediment P accumulation measured from the sediment core must be supplied by internal cycling, where the sediment core data accounts for the recent sediment accumulation rates but doesn't account for P mineralizing from deep sediments to the water column. We believe that this could be addressed with adjustments to the deep OP_{sed} pool. This shortcoming of the model will be addressed in future work.

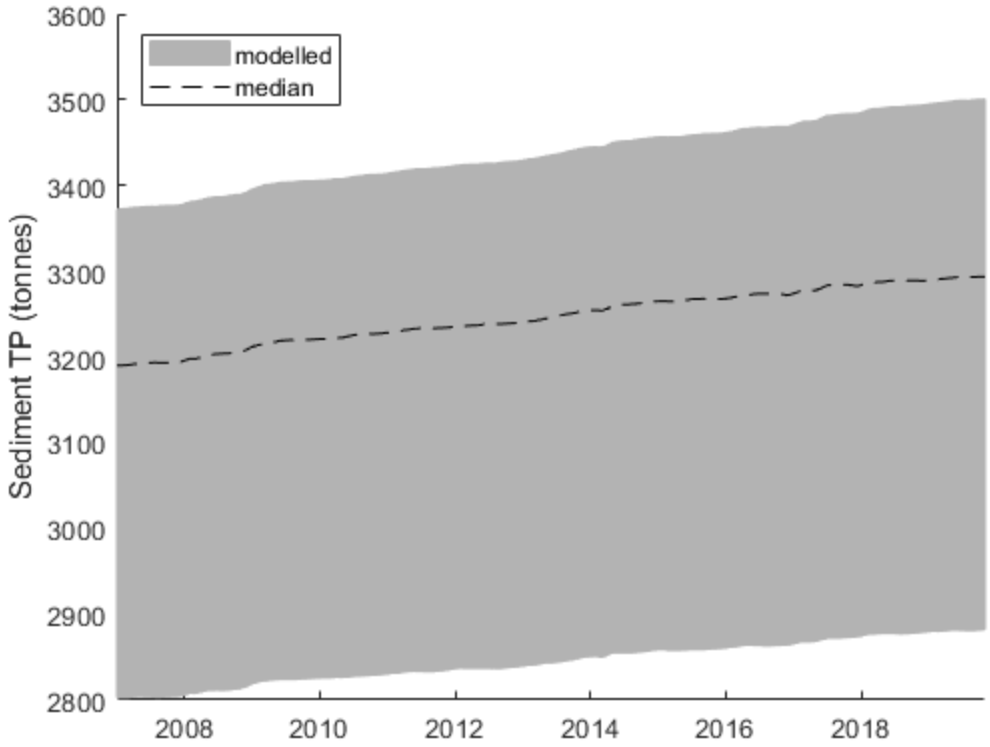

Figure 11. Modeled sediment TP accumulation between 2007 and 2019.

4.2.2 Model Results: Seasonal average fluxes between P pools

Next, I chose one parameter set to study the modeled average seasonal fluxes between P pools. The chosen parameter set had the best NSE_{SRP} and NSE_{TP}, 0.86 and 0.88 respectively. Using this parameter set, the resulting modeled average seasonal fluxes can confirm what we might expect to happen within the reservoir and can reveal internal cycling mechanisms. For example, we expect the SRP pool to be highest in the spring from external loading and then decrease in the summer when phytoplankton uptakes the supply, and the model reflects this (**Figure 12b and 12c**). As the phytoplankton use SRP in the summer, we expect the highest uptake flux in the summer, as uptake is dependent on temperature and available phosphate. The model captures this (**Figure 12c**). Since uptake is high in the summer, we expect elevated POP mass, where P is contained within phytoplankton, which is reflected by the model (**Figure 12c**).

As a rough check of the POP mass in the reservoir in the summer, I used some assumptions from the MyLake model that are used to relate phosphorus to chlorophyll

concentrations (Saloranta and Andersen 2007). Saloranta and Andersen (2007) assume that phytoplankton has a fixed Redfield composition (C:P = 106 by atoms, 40 by weight), and that this ratio is similar to the ratio of carbon to chlorophyll, implying an approximate yield coefficient of unity. These assumptions, in combination with our further assumption that most of the phosphorus within phytoplankton is in particulate organic form, imply that we can compare measured chlorophyll with modeled POP. Chlorophyll concentrations in Belwood Reservoir, measured in the summer of 1996, ranged from 0.8 µg/L to 25.4 µg/L (*Belwood and Conestogo Water Management Reservoirs* 2018). Using average summer reservoir volume, this translates to approximately 26 - 823 kg of POP in the water column in the summer. The amount of water-column POP in the summer is within reason when compared to this estimate. However, the modeled POP mass in the spring is likely incorrect since we would expect the POP pool to be greatest in the summer when phytoplankton is thriving. We suspect that the high spring POP is a result of the model trying to improve TP export performance, specifically the PP export. In reality, we think that less UPP would be settling in the spring when the reservoir is moreso acting as a flow-through system, and that this UPP should be supplying the PP export rather than POP. In fact, over all seasons the model underpredicts PP export. We believe that this is because the flux of UPP settling to sediment is too high, effectively saying that the reservoir is more of a sink than it actually is. This will be addressed in the future by potentially allowing the settling parameter to be seasonally-varying, or by imposing a lower upper-bound of the settling parameter.

In the fall when the phytoplankton dies, settling from the POP pool to the sediment OP pool is high (**Figure 12d**). Remobilization from the sediment is highest in the summer as expected with anoxic hypolimnetic release of legacy P (**Figure 12c**). This high remobilization from legacy P to SRP in the summer, in combination with the high septic inputs of SRP at the same time, likely contribute to the measured magnification of SRP:TP in the summer. Orihel et al (2017) reviewed internal P loading in 48 freshwater bodies in Canada, finding that gross internal loading rates ranged from -27 to 54 $mg/m^2/day$. In Belwood Reservoir, the modeled remobilization is 0.04561-0.05228 $mg/m^2/day$ on average, which is positive but low compared to the other lakes and reservoirs. This discrepancy suggests that there may be additional internal loading in Belwood Reservoir from legacy P that the model is not capturing at present. If the

model included the internal loading from legacy P stores, the modeled remobilization would be higher, closer to the values observed by Orihel et al (2017).

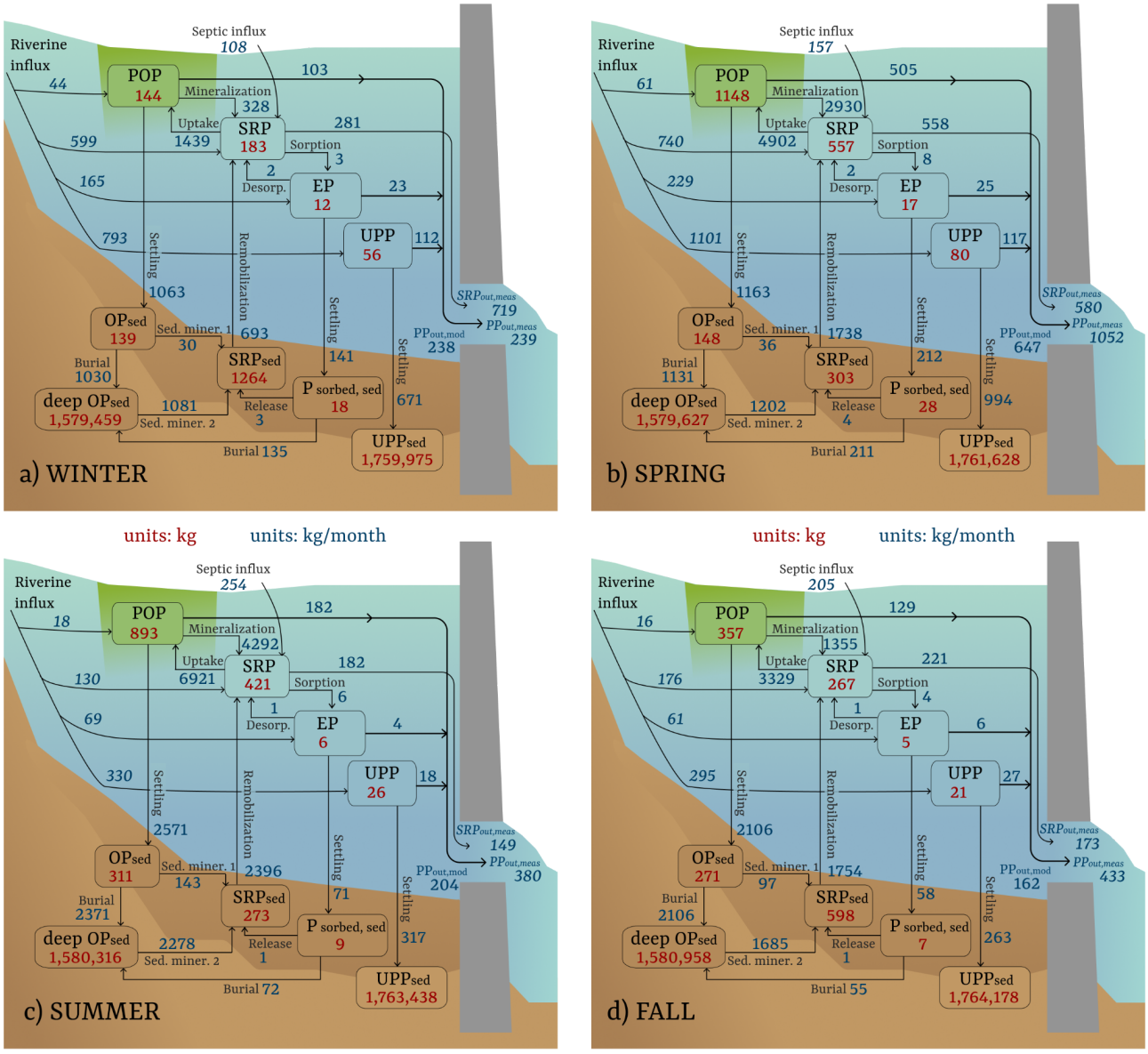

Figure 12. Average modeled seasonal fluxes between P pools, averaged between 2007-2019. Numbers in italics are measured.

4.3 Future Work

In the current state, the model is able to capture SRP and TP export dynamics at Belwood Reservoir quite well, and the SRP:TP magnification was captured for 2013-2019. In future work,

it would be interesting to divide the time period, calibrate the model parameters for each period, and then compare the calibrated parameter values. Alternatively, the decreasing trend in modeled SRP:TP magnification should be investigated since the data does not exhibit this temporal trend. Another shortcoming of the model was its underprediction of sediment P accumulation rate. We think that incorporation of sediment diagenesis processes in future iterations may be required to better capture the legacy P dynamics. Once the shortcomings of the model have been addressed, the model could be used to estimate when sediment P would be depleted and moreover, when the reservoir would stop seeing yearly algal blooms. Further, the model could be used to simulate the effect of climate or management changes on the occurrence of algal blooms.

5.0 Conclusions

For Research Objective 1, I quantified the effect of Belwood and Conestogo Reservoirs on seasonal P speciation. At the annual scale, Belwood and Conestogo Reservoirs fluctuated between acting as a source and a sink for SRP and TP. At Belwood and Conestogo Reservoirs in most years, the source-sink behaviour was consistent between SRP and TP at the annual scale. At Belwood Reservoir, the annual source-sink behaviour differed between SRP and TP in 5 of the 12 years (2008, 2012, 2016, 2018 and 2019), whereas the behaviour at Conestogo Reservoir only differed in 2 of the years (2015 and 2019). The ratio of SRP:TP was analyzed at the inlets and outlets of both reservoirs. At the seasonal scale, P loading regimes revealed that Belwood Reservoir acts as a sink for TP in March and April, and transitions to a source for June - October. This source/sink behaviour is driven by discharge relationships from March - April, whereas the behaviour is driven by a combination of discharge and concentration relationships in August - October. This magnification of the bioavailable P fraction has important consequences for downstream waters, as an increase in the bioavailable P fraction is often related to an increase in algal blooms (Watson et al. 2016). Both Belwood and Conestogo Reservoirs are a source of SRP through the summer, which is argued to be from a combination of summer stratification causing redox-related P release from lake sediment, and elevated septic contribution from cottages and camps surrounding the reservoirs. To analyze the relative fraction of bioavailable P, the monthly SRP:TP magnification from inlet to outlet was analyzed. The SRP:TP ratio is magnified by both reservoirs from May - August at Belwood Reservoir and April - September at Conestogo

Reservoir. Both reservoirs peak in magnification in July, where they are approximately doubling the proportion of bioavailable P along their respective streams.

For Research Objective 2, I created a process-based P model that simulates the speciation of P in the water column and lake sediment at the monthly scale. The model was calibrated to Belwood Reservoir and was able to capture SRP and TP export dynamics quite well (NSE_{SRP} = 0.57 - 0.86 and NSE_{TP} = 0.60 - 0.91). The magnification of SRP:TP from inlet to outlet was more difficult to capture (NSE_{mag} = -4.6 - 0.22), however the model appeared to have better performance in the latter half of the time period. The overall poor model performance of NSE_{mag} is due to the decreasing temporal trend over the full time period, which is something that should be investigated in the future. The model was not able to capture the legacy P accumulation to the expected magnitude, and we believe this could be fixed in the future with adjustments to the deep sediment organic P pool. In summary, both the study reservoirs altered P along their respective streams through P speciation and sediment-water P exchange, thus highlighting the impact of dams on downstream water quality. In future work, the sediment P accumulation rate will need to be improved so that the model can be used to simulate future scenarios and changes in climate and management.

References

Baker, D.B., Confesor, R., Ewing, D.E., Johnson, L.T., Kramer, J.W., and Merryfield, B.J. 2014. Phosphorus loading to Lake Erie from the Maumee, Sandusky and Cuyahoga rivers: The importance of bioavailability. Journal of Great Lakes Research, **40**: 502–517. doi:10.1016/j.jglr.2014.05.001.

Belwood and Conestogo Water Management Reservoirs: An Assessment of Surface and Groundwater Conditions. 2018. Grand River Conservation Authority. [accessed 15 September 2018].

Bennett, E.M., Carpenter, S.R., and Caraco, N.F. 2001. Human Impact on Erodable Phosphorus and Eutrophication: A Global Perspective: Increasing accumulation of phosphorus in soil threatens rivers, lakes, and coastal oceans with eutrophication. BioScience, **51**: 227–234. Oxford Academic. doi:10.1641/0006-3568(2001)051[0227:HIOEPA]2.0.CO;2.

Bolin, S.B., Ward, T.J., and Cole, R.A. 1987. Phosphorus Models Applied to New Mexico Reservoirs. Journal of Water Resources Planning and Management, **113**: 323–335. doi:10.1061/(ASCE)0733-9496(1987)113:3(323).

Boström, B., Jansson, M., and Forsberg, C. 1982. Phosphorus release from lake sediments. Arch. Hydrobiol., **18**: 5–59.

Boyd, D., and Shifflett, S. 2016. Low Flow Reliabilities in Regulated River Reaches in the Grand River Watershed. Grand River Conservation Authority, Cambridge, ON. Available from https://www.grandriver.ca/en/our-watershed/resources/Documents/WMP/GRCA-Reservoir-Yield-Tech-Report-May2016_FINAL.pdf.

Brzáková, M., Hejzlar, J., and Nedoma, J. 2003. Phosphorus uptake by suspended and settling seston in a stratified reservoir. Hydrobiologia, **504**: 39–49. doi:10.1023/B:HYDR.0000008506.29287.11.

Budd, J.W., Beeton, A.M., Stumpf, R.P., Culver, D.A., and Charles Kerfoot, W. 2001. Satellite observations of *Microcystis* blooms in western Lake Erie. SIL Proceedings, 1922-2010, **27**: 3787–3793. doi:10.1080/03680770.1998.11901692.

Canada, E. and C.C. 2007, January 9. Water Survey of Canada. program descriptions. Available from https://www.canada.ca/en/environment-climate-change/services/water-overview/quantity/monitoring/survey.html [accessed 22 March 2019].

Carpenter, S.R., Caraco, N.F., Correll, D.L., Howarth, R.W., Sharpley, A.N., and Smith, V.H. 1998. Nonpoint Pollution of Surface Waters with Phosphorus and Nitrogen. Ecological Applications, **8**: 559–568. doi:10.1890/1051-0761(1998)008[0559:NPOSWW]2.0.CO;2.

Compton, J., Mallinson, D., Glenn, C.R., Filippelli, G., Föllmi, K., Shields, G., and Zanin, Y. 2000. Variations in the Global Phosphorus Cycle. Available from http://archives.datapages.com/data/sepm_sp/SP66/Variations_in_the_Global_Phosphorus_Cycle.htm#purchaseoptions [accessed 27 March 2019].

Cordell, D., Drangert, J.-O., and White, S. 2009. The story of phosphorus: Global food security and food for thought. Global Environmental Change, **19**: 292–305. doi:10.1016/j.gloenvcha.2008.10.009.

De Pinto, J.V., Young, T.C., and McIlroy, L.M. 1986. Great lakes water quality improvement. Environmental Science & Technology, **20**: 752–759. American Chemical Society. doi:10.1021/es00150a001.

Dolan, D.M. 1993. Point Source Loadings of Phosphorus to Lake Erie: 1986–1990. Journal of

Great Lakes Research, **19**: 212–223. doi:10.1016/S0380-1330(93)71212-5.
Dolan, D.M., and McGunagle, K.P. 2005. Lake Erie Total Phosphorus Loading Analysis and Update: 1996–2002. Journal of Great Lakes Research, **31**: 11–22. doi:10.1016/S0380-1330(05)70301-4.
Donald, D.B., Parker, B.R., Davies, J.-M., and Leavitt, P.R. 2015. Nutrient sequestration in the Lake Winnipeg watershed. Journal of Great Lakes Research, **41**: 630–642. doi:10.1016/j.jglr.2015.03.007.
Ekholm, P., Malve, O., and Kirkkala, T. 1997. Internal and external loading as regulators of nutrient concentrations in the agriculturally loaded Lake Pyhäjärvi (southwest Finland). Hydrobiologia, **345**: 3–14. doi:10.1023/A:1002958727707.
Elser, J.J. 2012. Phosphorus: a limiting nutrient for humanity? Current Opinion in Biotechnology, **23**: 833–838. doi:10.1016/j.copbio.2012.03.001.
Gorham, E., and Boyce, F.M. 1989. Influence of Lake Surface Area and Depth Upon Thermal Stratification and the Depth of the Summer Thermocline. Journal of Great Lakes Research, **15**: 233–245. doi:10.1016/S0380-1330(89)71479-9.
Grand River Information Network. 2020. Available from https://data.grandriver.ca/ [accessed 13 January 2022].
GRCA. 2017. GRCA Landcover. Available from https://data.grandriver.ca/metadata/?id=2781 [accessed 19 June 2020].
Grill, G., Lehner, B., Lumsdon, A.E., MacDonald, G.K., Zarfl, C., and Liermann, C.R. 2015. An index-based framework for assessing patterns and trends in river fragmentation and flow regulation by global dams at multiple scales. Environmental Research Letters, **10**: 015001. IOP Publishing. doi:10.1088/1748-9326/10/1/015001.
Grimard, Y., and Jones, H.G. 1982. Trophic Upsurge in New Reservoirs: A Model for Total Phosphorus Concentrations. Canadian Journal of Fisheries and Aquatic Sciences, **39**: 1473–1483. doi:10.1139/f82-199.
Halemejko, G.Z., and Chrost, R.J. 1984. The role of phosphatases in phosphorus mineralization during decomposition of lake phytoplankton blooms. Arch. Hydrobiol., **101**: 489–502.
Hargreaves, G.H., and Samani, Z.A. 1985. Reference Crop Evapotranspiration from Temperature. Available from https://pubag.nal.usda.gov/catalog/5662005 [accessed 1 May 2020].
Hejzlar, J., Šámalová, K., Boers, P., and Kronvang, B. 2006. Modelling Phosphorus Retention in Lakes and Reservoirs. : 123–130. doi:10.1007/s11267-006-9032-7.
Hirsch, R.M., Moyer, D.L., and Archfield, S.A. 2010. Weighted Regressions on Time, Discharge, and Season (WRTDS), with an Application to Chesapeake Bay River Inputs. JAWRA Journal of the American Water Resources Association, **46**: 857–880. doi:10.1111/j.1752-1688.2010.00482.x.
Ho, J.C., Michalak, A.M., and Pahlevan, N. 2019. Widespread global increase in intense lake phytoplankton blooms since the 1980s. Nature, **574**: 667–670. Nature Publishing Group. doi:10.1038/s41586-019-1648-7.
Hondzo, M., and Stefan, H.G. 1991. Three Case Studies of Lake Temperature and Stratification Response to Warmer Climate. Water Resources Research, **27**: 1837–1846. doi:10.1029/91WR01281.
Hupfer, M., and Lewandowski, J. 2008. Oxygen Controls the Phosphorus Release from Lake Sediments – a Long-Lasting Paradigm in Limnology. International Review of Hydrobiology, **93**: 415–432. doi:10.1002/iroh.200711054.

International Joint Commission and International Joint Commission. 2014. A balanced diet for Lake Erie: reducing phosphorus loadings and harmful algal blooms. Available from http://www.deslibris.ca/ID/242490 [accessed 31 January 2020].

Jarvie, H.P., Sharpley, A.N., Spears, B., Buda, A.R., May, L., and Kleinman, P.J.A. 2013a. Water Quality Remediation Faces Unprecedented Challenges from "Legacy Phosphorus." Environmental Science & Technology, **47**: 8997–8998. American Chemical Society. doi:10.1021/es403160a.

Jarvie, H.P., Sharpley, A.N., Withers, P.J.A., Scott, J.T., Haggard, B.E., and Neal, C. 2013b. Phosphorus Mitigation to Control River Eutrophication: Murky Waters, Inconvenient Truths, and "Postnormal" Science. Journal of Environmental Quality, **42**: 295–304. The American Society of Agronomy, Crop Science Society of America, and Soil Science Society of America, Inc. doi:10.2134/jeq2012.0085.

Joosse, P.J., and Baker, D.B. 2011. Context for re-evaluating agricultural source phosphorus loadings to the Great Lakes. Canadian Journal of Soil Science, **91**: 317–327. NRC Research Press. doi:10.4141/cjss10005.

Kane, D.D., Conroy, J.D., Peter Richards, R., Baker, D.B., and Culver, D.A. 2014. Re-eutrophication of Lake Erie: Correlations between tributary nutrient loads and phytoplankton biomass. Journal of Great Lakes Research, **40**: 496–501. doi:10.1016/j.jglr.2014.04.004.

Katsev, S., Tsandev, I., L'Heureux, I., and Rancourt, D.G. 2006. Factors controlling long-term phosphorus efflux from lake sediments: Exploratory reactive-transport modeling. Chemical Geology, **234**: 127–147. doi:10.1016/j.chemgeo.2006.05.001.

Ku, A., DiGianol, F., and Feng, T. 1978. Factors affecting phosphate adsorption equilibria in lake sediments.

Labry, C., Youenou, A., Delmas, D., and Michelon, P. 2013. Addressing the measurement of particulate organic and inorganic phosphorus in estuarine and coastal waters. Continental Shelf Research, **60**: 28–37. doi:10.1016/j.csr.2013.04.019.

Loomer, H.A., and Cooke, S.E. 2011. Water quality in the Grand River Watershed: Current Conditions & Trends (2003-2008). Grand River Conservation Authority. Available from https://www.sourcewater.ca/en/source-protection-areas/resources/Documents/Grand/Grand_Reports_WaterQuality_2011.pdf.

Maavara, T., Chen, Q., Van Meter, K., Brown, L.E., Zhang, J., Ni, J., and Zarfl, C. 2020. River dam impacts on biogeochemical cycling. Nature Reviews Earth & Environment, **1**: 103–116. Nature Publishing Group. doi:10.1038/s43017-019-0019-0.

Maavara, T., Parsons, C.T., Ridenour, C., Stojanovic, S., Dürr, H.H., Powley, H.R., and Van Cappellen, P. 2015. Global phosphorus retention by river damming. Proceedings of the National Academy of Sciences,: 201511797. doi:10.1073/pnas.1511797112.

Magee, M.R., Wu, C.H., Robertson, D.M., Lathrop, R.C., and Hamilton, D.P. 2016. Trends and abrupt changes in 104 years of ice cover and water temperature in a dimictic lake in response to air temperature, wind speed, and water clarity drivers. Hydrology and Earth System Sciences, **20**: 1681–1702. doi:10.5194/hess-20-1681-2016.

Makarewicz, J.C., and Bertram, P. 1991. Evidence for the Restoration of the Lake Erie EcosystemWater quality, oxygen levels, and pelagic function appear to be improving. BioScience, **41**: 216–223. Oxford Academic. doi:10.2307/1311411.

Matott, L.S. 2017. OSTRICH: An Optimization Software Tool, Documentation and User's Guide, Version 17.12.19. University of Buffalo Center for Computational Research.

Available from http://www.civil.uwaterloo.ca/envmodelling/Ostrich.html.
Mccombie, A.M. 1959. Some Relations Between Air Temperatures and the Surface Water Temperatures of Lakes. Limnology and Oceanography, **4**: 252–258. doi:https://doi.org/10.4319/lo.1959.4.3.0252.
Meybeck, M. 1993. C, N, P and S in Rivers: From Sources to Global Inputs. *In* Interactions of C, N, P and S Biogeochemical Cycles and Global Change. *Edited by* R. Wollast, F.T. Mackenzie, and L. Chou. Springer Berlin Heidelberg. pp. 163–193.
Michalak, A.M., Anderson, E.J., Beletsky, D., Boland, S., Bosch, N.S., Bridgeman, T.B., Chaffin, J.D., Cho, K., Confesor, R., Daloğlu, I., DePinto, J.V., Evans, M.A., Fahnenstiel, G.L., He, L., Ho, J.C., Jenkins, L., Johengen, T.H., Kuo, K.C., LaPorte, E., Liu, X., McWilliams, M.R., Moore, M.R., Posselt, D.J., Richards, R.P., Scavia, D., Steiner, A.L., Verhamme, E., Wright, D.M., and Zagorski, M.A. 2013. Record-setting algal bloom in Lake Erie caused by agricultural and meteorological trends consistent with expected future conditions. Proceedings of the National Academy of Sciences, **110**: 6448–6452. National Academy of Sciences. doi:10.1073/pnas.1216006110.
Molot, L.A., Watson, S.B., Creed, I.F., Trick, C.G., McCabe, S.K., Verschoor, M.J., Sorichetti, R.J., Powe, C., Venkiteswaran, J.J., and Schiff, S.L. 2014. A novel model for cyanobacteria bloom formation: the critical role of anoxia and ferrous iron. Freshwater Biology, **59**: 1323–1340. doi:10.1111/fwb.12334.
Muenich, R.L., Kalcic, M., and Scavia, D. 2016. Evaluating the Impact of Legacy P and Agricultural Conservation Practices on Nutrient Loads from the Maumee River Watershed. Environmental Science & Technology, **50**: 8146–8154. American Chemical Society. doi:10.1021/acs.est.6b01421.
Nash, J.E., and Sutcliffe, J.V. 1970. River flow forecasting through conceptual models part I — A discussion of principles. Journal of Hydrology, **10**: 282–290. doi:10.1016/0022-1694(70)90255-6.
Nürnberg, G.K. 1984. The prediction of internal phosphorus load in lakes with anoxic hypolimnia. Limnology and Oceanography, **29**: 111–124. doi:10.4319/lo.1984.29.1.0111.
Nürnberg, G.K. 2009. Assessing internal phosphorus load – Problems to be solved. Lake and Reservoir Management, **25**: 419–432. Taylor & Francis. doi:10.1080/00357520903458848.
Orihel, D.M., Baulch, H.M., Casson, N.J., North, R.L., Parsons, C.T., Seckar, D.C.M., and Venkiteswaran, J.J. 2017. Internal phosphorus loading in Canadian fresh waters: a critical review and data analysis. Canadian Journal of Fisheries and Aquatic Sciences, **74**: 2005–2029. doi:10.1139/cjfas-2016-0500.
Ouellette, A.J.A., Handy, S.M., and Wilhelm, S.W. 2006. Toxic Microcystis is Widespread in Lake Erie: PCR Detection of Toxin Genes and Molecular Characterization of Associated Cyanobacterial Communities. Microbial Ecology, **51**: 154–165. doi:10.1007/s00248-004-0146-z.
Paerl, H.W. 1988. Nuisance phytoplankton blooms in coastal, estuarine, and inland waters. Limnology and Oceanography, **33**: 823–843. doi:10.4319/lo.1988.33.4part2.0823.
Paerl, H.W., Hall, N.S., and Calandrino, E.S. 2011. Controlling harmful cyanobacterial blooms in a world experiencing anthropogenic and climatic-induced change. Science of The Total Environment, **409**: 1739–1745. doi:10.1016/j.scitotenv.2011.02.001.
Pettersson, K. 1998. Mechanisms for internal loading of phosphorus in lakes. Hydrobiologia, **373**: 21–25. doi:10.1023/A:1017011420035.

Porcalová, P. 1990. Phosphorus Losses from the Epilimnion in Římov Reservoir. Internationale Revue der gesamten Hydrobiologie und Hydrographie, **75**: 273–279. doi:10.1002/iroh.19900750302.

Powers, S.M., Robertson, D.M., and Stanley, E.H. 2013. Effects of lakes and reservoirs on annual river nitrogen, phosphorus, and sediment export in agricultural and forested landscapes. Hydrological Processes, **28**: 5919–5937. doi:10.1002/hyp.10083.

Powers, S.M., Tank, J.L., and Robertson, D.M. 2015. Control of nitrogen and phosphorus transport by reservoirs in agricultural landscapes. Biogeochemistry, **124**: 417–439. doi:10.1007/s10533-015-0106-3.

Richards, R.P., Baker, D.B., Crumrine, J.P., and Stearns, A.M. 2010. Unusually large loads in 2007 from the Maumee and Sandusky Rivers, tributaries to Lake Erie. Journal of Soil and Water Conservation, **65**: 450–462. Soil and Water Conservation Society. doi:10.2489/jswc.65.6.450.

Rigler, F.H. 1956. A Tracer Study of the Phosphorus Cycle in Lake Water. Ecology, **37**: 550–562. Ecological Society of America. doi:10.2307/1930179.

Rigler, F.H. 1964. The Phosphorus Fractions and the Turnover Time of Inorganic Phosphorus in Different Types of Lakes,1. Limnology and Oceanography, **9**: 511–518. doi:10.4319/lo.1964.9.4.0511.

Saloranta, T.M., and Andersen, T. 2007. MyLake—A multi-year lake simulation model code suitable for uncertainty and sensitivity analysis simulations. Ecological Modelling, **207**: 45–60. Elsevier. doi:10.1016/j.ecolmodel.2007.03.018.

Salvia-Castellvi, M., Dohet, A., Vander Borght, P., and Hoffmann, L. 2001. Control of the eutrophication of the reservoir of Esch-sur-Sûre (Luxembourg): evaluation of the phosphorus removal by predams. Hydrobiologia, **459**: 61–71. doi:10.1023/A:1012548006413.

Scavia, D., David Allan, J., Arend, K.K., Bartell, S., Beletsky, D., Bosch, N.S., Brandt, S.B., Briland, R.D., Daloğlu, I., DePinto, J.V., Dolan, D.M., Evans, M.A., Farmer, T.M., Goto, D., Han, H., Höök, T.O., Knight, R., Ludsin, S.A., Mason, D., Michalak, A.M., Peter Richards, R., Roberts, J.J., Rucinski, D.K., Rutherford, E., Schwab, D.J., Sesterhenn, T.M., Zhang, H., and Zhou, Y. 2014. Assessing and addressing the re-eutrophication of Lake Erie: Central basin hypoxia. Journal of Great Lakes Research, **40**: 226–246. doi:10.1016/j.jglr.2014.02.004.

Schindler, D.W., Carpenter, S.R., Chapra, S.C., Hecky, R.E., and Orihel, D.M. 2016. Reducing Phosphorus to Curb Lake Eutrophication is a Success. Environmental Science & Technology, **50**: 8923–8929. doi:10.1021/acs.est.6b02204.

Sharpley, A., Jarvie, H.P., Buda, A., May, L., Spears, B., and Kleinman, P. 2013. Phosphorus Legacy: Overcoming the Effects of Past Management Practices to Mitigate Future Water Quality Impairment. Journal of Environmental Quality, **42**: 1308–1326. doi:10.2134/jeq2013.03.0098.

Shaughnessy, A.R., Sloan, J.J., Corcoran, M.J., and Hasenmueller, E.A. 2019. Sediments in Agricultural Reservoirs Act as Sinks and Sources for Nutrients over Various Timescales. Water Resources Research, **0**. doi:10.1029/2018WR024004.

Song, K., Adams, C.J., and Burgin, A.J. 2017. Relative importance of external and internal phosphorus loadings on affecting lake water quality in agricultural landscapes. Ecological Engineering, **108**: 482–488. doi:10.1016/j.ecoleng.2017.06.008.

Song, K., and Burgin, A.J. 2017. Perpetual Phosphorus Cycling: Eutrophication Amplifies

Biological Control on Internal Phosphorus Loading in Agricultural Reservoirs. Ecosystems, **20**: 1483–1493. doi:10.1007/s10021-017-0126-z.

State of the Watershed Report. 1998. Available from https://www.grandriver.ca/en/our-watershed/resources/Documents/Water_History_1998HealthReport.pdf.

Watson, S.B., Miller, C., Arhonditsis, G., Boyer, G.L., Carmichael, W., Charlton, M.N., Confesor, R., Depew, D.C., Höök, T.O., Ludsin, S.A., Matisoff, G., McElmurry, S.P., Murray, M.W., Peter Richards, R., Rao, Y.R., Steffen, M.M., and Wilhelm, S.W. 2016. The re-eutrophication of Lake Erie: Harmful algal blooms and hypoxia. Harmful Algae, **56**: 44–66. doi:10.1016/j.hal.2016.04.010.

Wetzel, R.G. (*Editor*). 1983. Periphyton of Freshwater Ecosystems: Proceedings of the First International Workshop on Periphyton of Freshwater Ecosystems held in Växjö, Sweden, 14–17 September 1982. Springer Netherlands. doi:10.1007/978-94-009-7293-3.

Winton, R.S., Calamita, E., and Wehrli, B. 2019. Reviews and syntheses: Dams, water quality and tropical reservoir stratification. Biogeosciences, **16**: 1657–1671. doi:https://doi.org/10.5194/bg-16-1657-2019.

Woolway, R.I., and Merchant, C.J. 2019. Worldwide alteration of lake mixing regimes in response to climate change. Nature Geoscience, **12**: 271. doi:10.1038/s41561-019-0322-x.

Yuan, Z., Jiang, S., Sheng, H., Liu, X., Hua, H., Liu, X., and Zhang, Y. 2018. Human Perturbation of the Global Phosphorus Cycle: Changes and Consequences. Environmental Science & Technology, **52**: 2438–2450. American Chemical Society. doi:10.1021/acs.est.7b03910.

Appendix

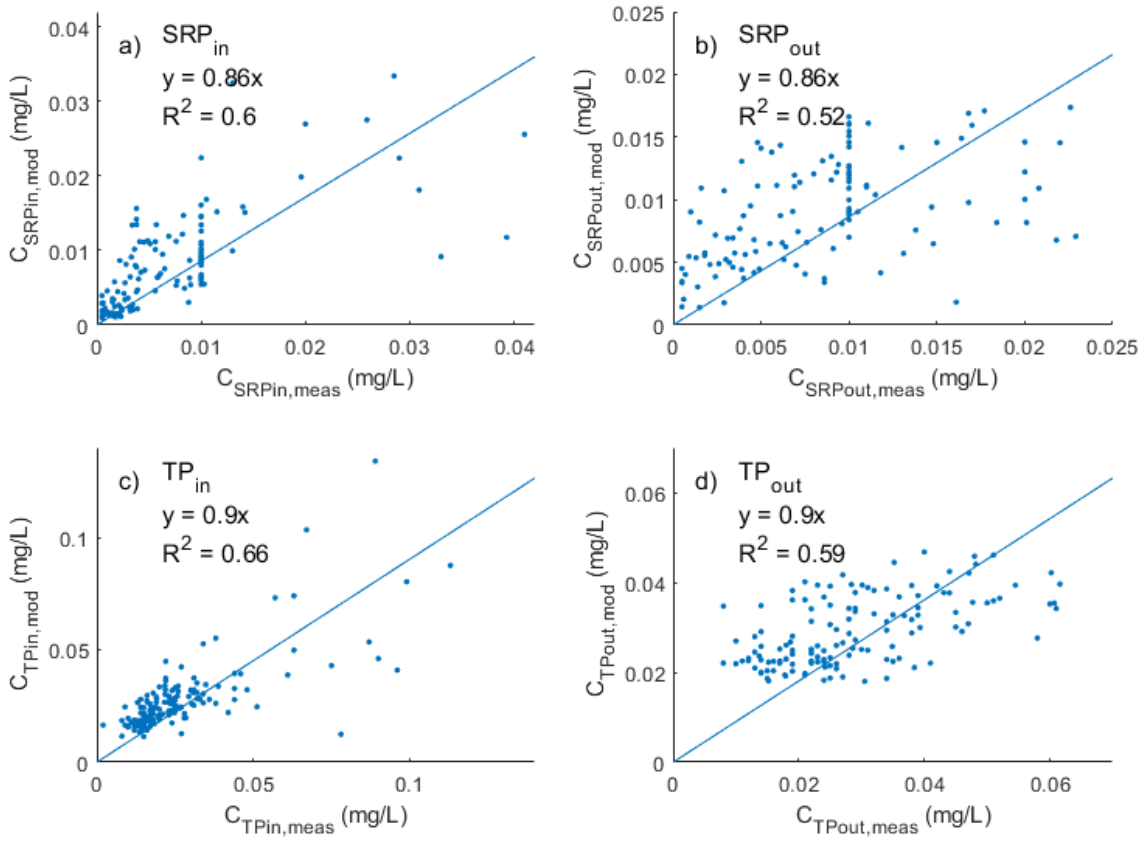

Figure 13. Measured and WRTDS-modeled SRP and TP concentrations for inlet and outlet of Belwood Reservoir.

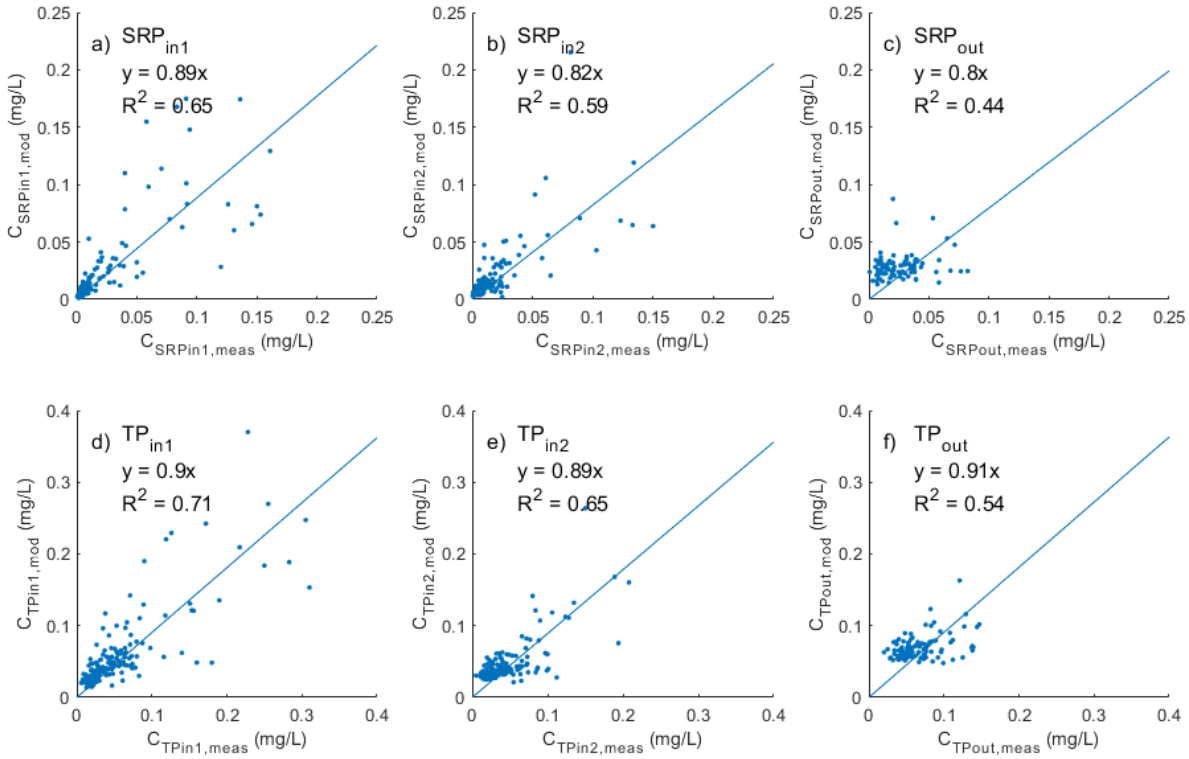

Figure 14. Measured and WRTDS-modeled SRP and TP concentrations for inlets and outlet of Conestogo Reservoir.

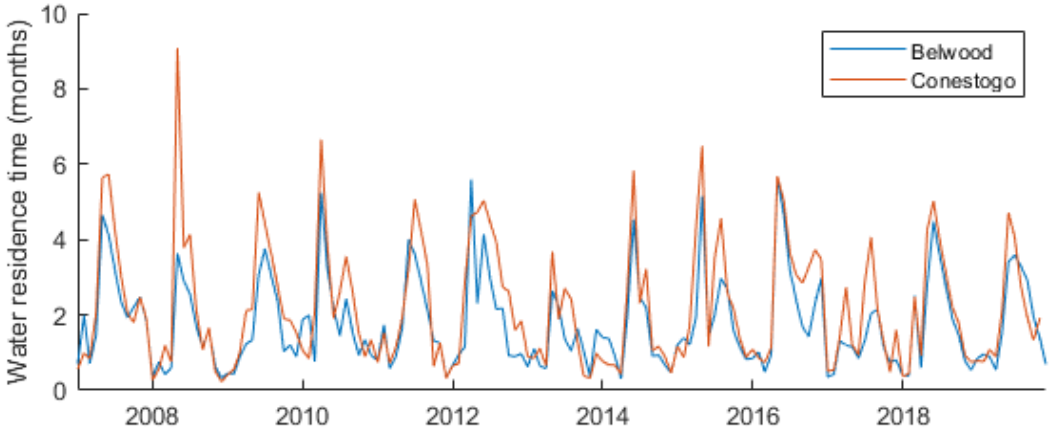

Figure 15. Monthly water residence times in Belwood and Conestogo Reservoirs.

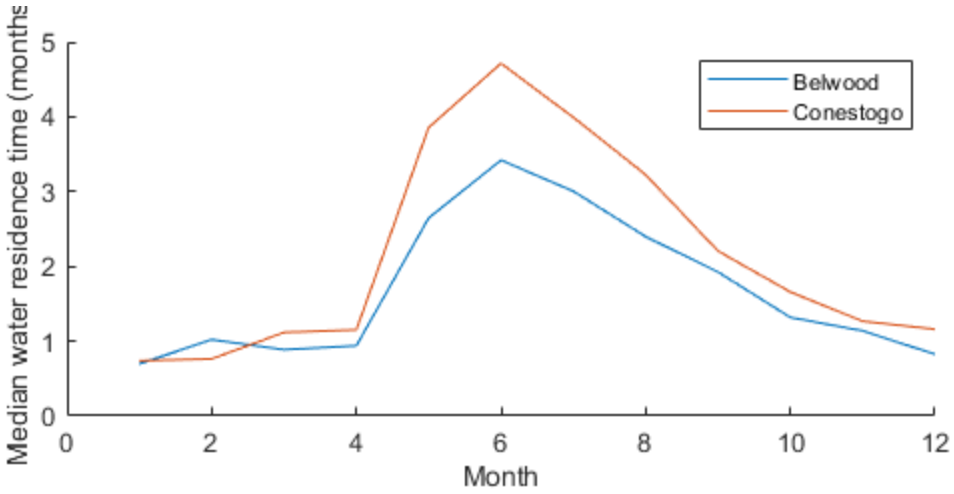

Figure 16. Monthly median water residence times in Belwood and Conestogo Reservoirs.

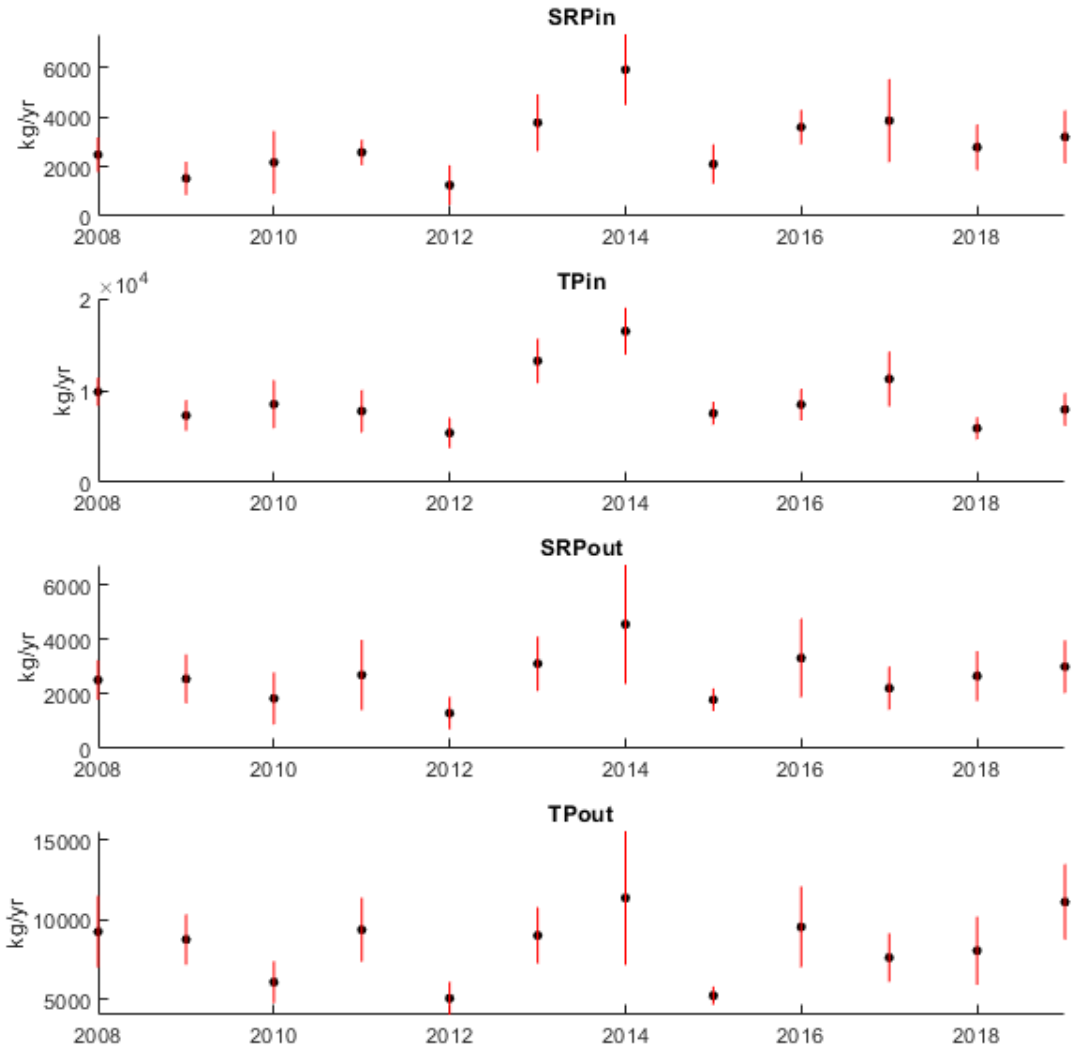

Figure 17. Annual fluxes at Belwood Reservoir with respective confidence intervals.

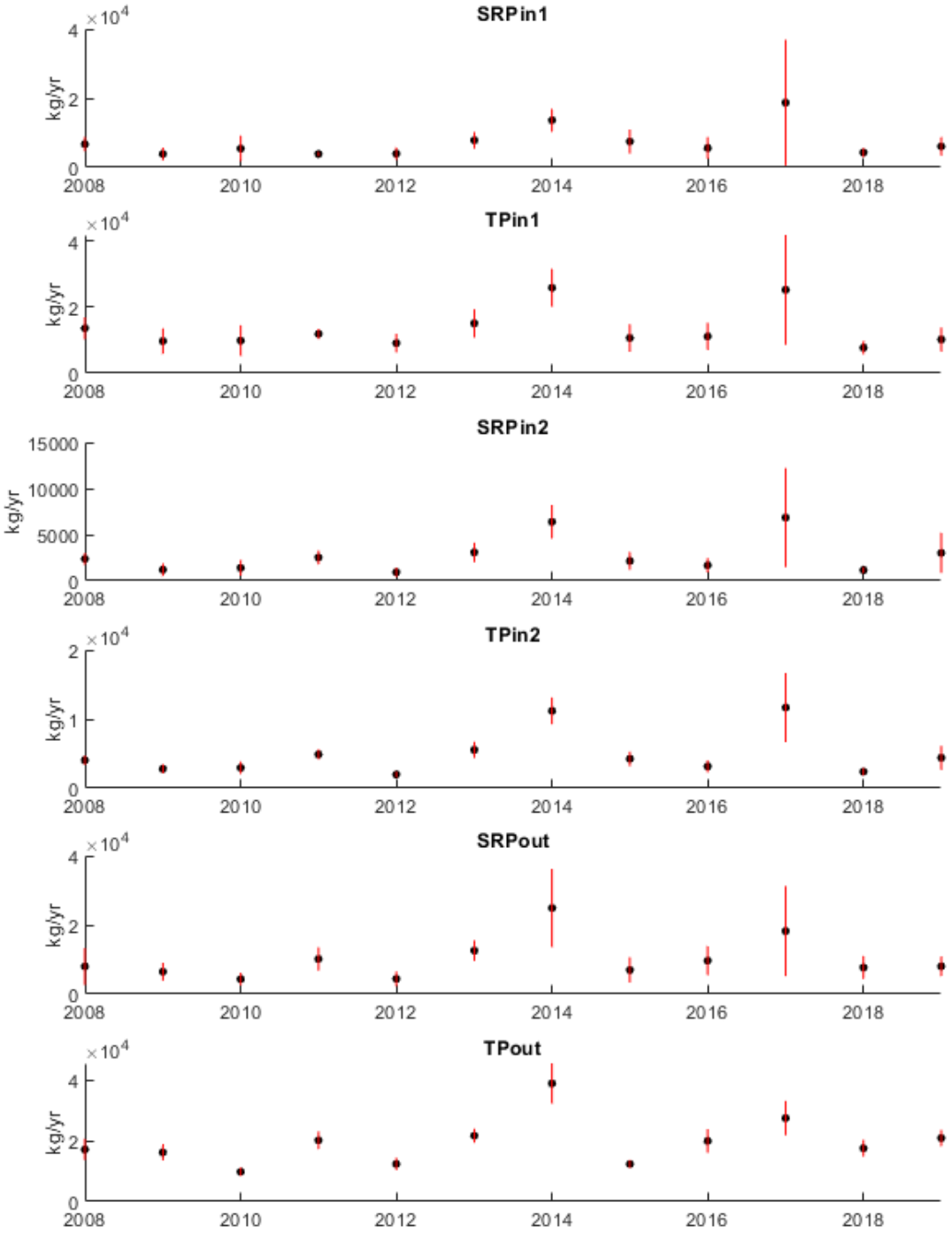

Figure 18. Annual fluxes at Conestogo Reservoir with respective confidence intervals.

Code snippet - main script: res.m


```
% This script uses RK4 to solve the 9 coupled equations for species of P
%   in the water column and sediment of Belwood Reservoir.
%   Calls on the functions f.m and calc_error_metrics.m
% The model is run at the sub-monthly scale of 1000 time steps per month.
% After the state variable matrix has been estimated at this scale, monthly
% estimates are calculated as the average over the 1000 time steps.
%   Inputs: Time series of SRP and TP riverine loading, reservoir volume, air temp, and
%           outlet discharge, which are loaded from model_inputs_bel.mat. The script
%           reads the parameter set from res_calibration_input_bel.txt, where this
%           file is an output of using OSTRICH (Matott 2017).
%   Output: P_mon is a matrix of the monthly-averaged mass (kg) in each of the 9 pools
clear

load 'model_inputs_bel.mat'

%% RK4 initialization
num_pools = 9; % total number of pools
num_wc_pools = 4; % water-column pools


% P = [SRP; POP; EP; UPP; SRPsed; OPsed; SorbedPsed; UPPsed; deep OPsed];
% See Table 3 for description of state variables and see Section 3.3.1
% for details on estimation of initial conditions
P = zeros(num_pools,ts); % state variables time series matrix
P(:,1) = [44;20;354;74; 2925000*0.27; 2925000*0.03; ...
    2925000*0.12; 2925000*0.58; 5850000];  % IC for 2007


% Load parameter set from text file
param_set = table2array(readtable('res_calibration_input_bel.txt',...
    'FileType','text','Delimiter','space','MultipleDelimsAsOne',true));

constants = [alpha_POP, alpha_EP, alpha_UPP, dt];
model_inputs = [airT, Q_out, V, SRP_in, TP_in];


%% Run RK4

for t = 1:ts-1

    k1 = dt*f_of_tandP( t, P(:,t), param_set, constants, model_inputs );  % tn,yn
    k2 = dt*f_of_tandP( t+0.5*dt, P(:,t)+0.5*k1, param_set, constants, model_inputs ); %↙
tn+0.5*h
    k3 = dt*f_of_tandP( t+0.5*dt, P(:,t)+0.5*k2, param_set, constants, model_inputs ); %↙
tn+0.5*h
    k4 = dt*f_of_tandP( t+dt, P(:,t)+k3, param_set, constants, model_inputs ); % tn+h

    P(:,t+1) = P(:,t) + 1/6*(k1 + 2*k2 + 2*k3 + k4);

end
```

```
%% Calculate monthly values

P_mon = zeros(num_pools,mons);
for t = 1:mons
    startIdx = (t-1)*(1/dt)+1;
    endIdx = t/dt;
    P_mon(:,t) = mean(P(:,startIdx:endIdx),2);
end
```

Code snippet: helper function: f_of_tandP.m


```
function [f_k] = f_of_tandP(t, P, param_set, constants, model_inputs)
% This function calculates the pool masses at the next time step using the
% DEs as defined below. For non-integer times (for example, when calculating
% k2 and k3), a linear approximation of the input between two known times is used.
% The function takes the input time, t, and sets the seasonal parameters accordingly.
% Mineralization and uptake rates are calculated as a function of water temperature
% (which is inferred from measured air temperature), and uptake rate also depends on
% phosphate (SRP) saturation. Septic contribution is also calculated depending
% on the month.
%    Inputs: time t, vector of state variables P, a vector of all parameters
%            param_set, alphas for proportioning incoming particulate P, time
%            step size dt, vectors of air temp, outflow, reservoir volume,
%            and inlet fluxes of SRP and TP.
%    Output: a vector, f_k, of the state variables at t and P

%% Rename values for readability

    % Parameters - refer to Table 4
    k_sorp = param_set(1);
    k_desorp = param_set(2);
    p_prop_exp = param_set(3);
    m20 = param_set(4);
    mu20 = param_set(5);
    Pd_prime = param_set(6);
    k_remob_summ = param_set(7);
    k_remob_wint = param_set(8);
    k_remob_spr = param_set(9);
    k_remob_fall = param_set(10);
    k_sett = param_set(11);
    k_sett_pop_summ = param_set(12);
    k_sett_pop_wint = param_set(13);
    k_sett_pop_spr = param_set(14);
    k_sett_pop_fall = param_set(15);
    m20_sed1 = param_set(16);
    m20_sed2 = param_set(17);
    k_bur = param_set(18);
    k_sed_release = param_set(19);
    k_sed_release_summ = param_set(20);

    % Constants - see Section 3.3.1 for explanation of alphas
    alpha_POP = constants(1);
    alpha_EP = constants(2);
    alpha_UPP = constants(3);
    dt = constants(4); % 0.001 month

    % Input vectors - see Section 3.3.1
    airT = model_inputs(:,1); % deg C
    Q_out = model_inputs(:,2); % m3/month
    V = model_inputs(:,3); % m3
    SRP_in = model_inputs(:,4); % kg/month
    TP_in = model_inputs(:,5); % kg/month
```

```
%%  Linear approx of values at non-integer times

    t1 = floor(t);
    t2 = ceil(t);

    m = TP_in(t2) - TP_in(t1);
    TPin = TP_in(t1) + m*(t-t1);

    m = SRP_in(t2) - SRP_in(t1);
    SRPin = SRP_in(t1) + m*(t-t1);

    PPin = TPin - SRPin;

    m = V(t2) - V(t1);
    Vt = V(t1) + m*(t-t1);

    m = Q_out(t2) - Q_out(t1);
    Qt = Q_out(t1) + m*(t-t1);

%% Set the seasonal parameters based on time

    if mod(t1,12/dt)<=2/dt || mod(t1,12/dt)>11/dt % Dec-Feb
        k_remob = k_remob_wint;
        k_sett_pop = k_sett_pop_wint;

    elseif mod(t1,12/dt)<=5/dt && mod(t1,12/dt)>2/dt % Mar-May
        k_remob = k_remob_spr;
        k_sett_pop = k_sett_pop_spr;

    elseif mod(t1,12/dt)<=8/dt && mod(t1,12/dt)>5/dt % Jun-Aug
        k_remob = k_remob_summ;
        k_sed_release = k_sed_release_summ;
        k_sett_pop = k_sett_pop_summ;

    else  % Sept-Nov
        k_remob = k_remob_fall;
        k_sett_pop = k_sett_pop_fall;

    end

%% Calculate uptake and mineralization using MyLake equations
%    Eqns 26 and 27 from (Saloranta and Andersen 2007)
%    Since both equations are temperature dependent, infer water temps
%    from measured air temp (McCombie 1959):
%        water temp = m*(air temp) + b, where in
%            May, June, July: m = 1.01, b = -9
%            Aug, Sept, Oct, Nov: m = 0.714, b = +0.3
%    Water temp in winter assumed to be 1.5 deg C (Magee et al 2016)

theta = exp(0.1*log(2)); % assumes Q10 = 2
```

```
dpm = 30.4; % average days per month

if mod(t1,12/dt) <= 7/dt && mod(t1,12/dt) > 4/dt % May-July

    waterT = 1.01*airT(t1) - 9;
    k_miner = m20*theta^(waterT-20);
    k_miner = k_miner*dpm; % 1/day to 1/mon

    k_sed_miner = m20_sed1*theta^(waterT-20);
    k_sed_miner = k_sed_miner*dpm;
    k_sed_miner2 = m20_sed2*theta^(waterT-20);
    k_sed_miner2 = k_sed_miner2*dpm;

elseif mod(t1,12/dt) <= 11/dt && mod(t1,12/dt) > 7/dt % Aug-Nov

    waterT = 0.714*airT(t1) + 0.3;
    Pd = P(1)/Vt*1e6; % SRP in mg/m3
    muT = mu20*theta^(waterT-20); % 1/day
    k_up = muT*Pd/(Pd_prime+Pd); % 1/day
    k_up = k_up*dpm;

    k_miner = m20*theta^(waterT-20);
    k_miner = k_miner*dpm;

    k_sed_miner = m20_sed1*theta^(waterT-20);
    k_sed_miner = k_sed_miner*dpm;
    k_sed_miner2 = m20_sed2*theta^(waterT-20);
    k_sed_miner2 = k_sed_miner2*dpm;

else % Dec-Apr

    waterT = 1.5; % deg C est from Magee et al 2016 (1-2 ish deg C)

    Pd = P(1)/Vt*1e6; % SRP in mg/m3
    muT = mu20*theta^(waterT-20); % 1/day
    k_up = muT*Pd/(Pd_prime+Pd); % 1/day
    k_up = k_up*dpm;

    k_miner = m20*theta^(waterT-20);
    k_miner = k_miner*dpm;

    k_sed_miner = m20_sed1*theta^(waterT-20);
    k_sed_miner = k_sed_miner*dpm;
    k_sed_miner2 = m20_sed2*theta^(waterT-20);
    k_sed_miner2 = k_sed_miner2*dpm;

end

%% Calculate septic system inputs depending on the month

if mod(t1,12/dt) <= 10/dt && mod(t1,12/dt) > 4/dt % May-Oct
```

```
    SRPin_septic = 876.4/6 + 1295/12; %kg

else % Oct-Apr
    SRPin_septic = 1295/12;

end

    %% Solve system of DEs

    f_k = zeros(8,1);

    % SRP soluble reactive P
    f_k(1) = SRPin_septic + SRPin + k_miner*P(2) + k_desorp*P(3) + k_remob*P(5) ...
              - k_up*P(1) - k_sorp*P(1) - Qt*P(1)/Vt;

    % POP particulate organic P
    f_k(2) = PPin*alpha_POP/(alpha_POP+alpha_EP+alpha_UPP) + k_up*P(1) ...
              - k_miner*P(2) - k_sett_pop*P(2) - p_prop_exp*Qt*P(2)/Vt;

    % EP exchangeable P
    f_k(3) = PPin*alpha_EP/(alpha_POP+alpha_EP+alpha_UPP) + k_sorp*P(1) ...
              - k_desorp*P(3) - k_sett*P(3) - Qt*P(3)/Vt;

    % UPP unreactive particulate P
    f_k(4) = PPin*alpha_UPP/(alpha_POP+alpha_EP+alpha_UPP) - k_sett*P(4) - Qt*P(4)/Vt;

    % Porewater SRP in sediment
    f_k(5) = k_sed_miner*P(6) + k_sed_release*P(7) + k_sed_miner2*P(9) - k_remob*P(5);

    % OP in sediment
    f_k(6) = k_sett_pop*P(2) - k_sed_miner*P(6) - k_bur*P(6);

    % Sorbed P in sediment
    f_k(7) = k_sett*P(3) - k_sed_release*P(7) - k_bur*P(7);

    % UPP in sediment
    f_k(8) = k_sett*P(4);

    % Deep OP in sediment
    f_k(9) = k_bur*P(6) + k_bur*P(7) - k_sed_miner2*P(9);


end
```